Early Astrocytic Dysfunction Is Associated with Mistuned Synapses as well as Anxiety and Depressive-Like Behavior in the App^{NL-F} Mouse Model of Alzheimer's Disease

Benjamin Portal[a], Moa Södergren[a], Teo Parés i Borrell[a], Romain Giraud[a], Nicole G. Metzendorf[b], Greta Hultqvist[b], Per Nilsson[c] and Maria Lindskog[a,c,*]

[a]*Department for Medical Cell Biology, Uppsala University, Uppsala, Sweden*
[b]*Department of Pharmacy, Division of Protein Drug Design, Uppsala University, Uppsala, Sweden*
[c]*Department of Neurobiology, Care Sciences and Society, Division of Neurogeriatrics, Center for Alzheimer Research, Karolinska Institutet, Stockholm, Sweden*

Abstract.
Background: Alzheimer's disease (AD) is the most common neurodegenerative disease. Unfortunately, efficient and affordable treatments are still lacking for this neurodegenerative disorder, it is therefore urgent to identify new pharmacological targets. Astrocytes are playing a crucial role in the tuning of synaptic transmission and several studies have pointed out severe astrocyte reactivity in AD. Reactive astrocytes show altered physiology and function, suggesting they could have a role in the early pathophysiology of AD.
Objective: We aimed to characterize early synaptic impairments in the App^{NL-F} knock-in mouse model of AD, especially to understand the contribution of astrocytes to early brain dysfunctions.
Methods: The App^{NL-F} mouse model carries two disease-causing mutations inserted in the amyloid precursor protein gene. This strain does not start to develop amyloid-β plaques until 9 months of age. Thanks to electrophysiology, we investigated synaptic function, at both neuronal and astrocytic levels, in 6-month-old animals and correlate the synaptic activity with emotional behavior.
Results: Electrophysiological recordings in the hippocampus revealed an overall synaptic mistuning at a pre-plaque stage of the pathology, associated to an intact social memory but a stronger depressive-like behavior. Astrocytes displayed a reactive-like morphology and a higher tonic GABA current compared to control mice. Interestingly, we here show that the synaptic impairments in hippocampal slices are partially corrected by a pre-treatment with the monoamine oxidase B blocker deprenyl or the fast-acting antidepressant ketamine (5 mg/kg).
Conclusions: We propose that reactive astrocytes can induce synaptic mistuning early in AD, before plaques deposition, and that these changes are associated with emotional symptoms.

Keywords: Alzheimer's disease, *App* knock-in mice, depression, LTP, MAO-B, synapse

*Correspondence to: Maria Lindskog, Department for Medical Cell Biology, Uppsala University, Box 571, 751 23 Uppsala, Sweden. E-mail: Mia.Lindskog@uu.se.

INTRODUCTION

Alzheimer's disease (AD) is a progressive age-related neurodegenerative disorder accounting for 75% of dementia cases worldwide [1]. Patients show significant memory loss [2] together with multiple secondary symptoms such as social isolation [3] and depressive symptoms [4]. In recent years, significant improvements have been done in clinical care of patients and recent anti-amyloid-β (Aβ) immunotherapies have shown promising results in early phases of the pathology [5]. However, the underlaying mechanisms of this pathology are still unknown. Intracellular tau neurofibrillary tangles [6] and Aβ aggregation [7] are the main molecular hallmarks of the pathology and have been given considerable attention in the attempt to understand the disorder. Extensive cellular rearrangements occur around Aβ plaques, including synaptic degeneration and astrocyte reactivity. In addition, Aβ can take other aggregated forms, including oligomers that are known to deteriorate neuronal activity [8] and affect astrocytic secretome [9], and has been suggested to have an even stronger adverse effect than Aβ plaques on neuronal and astrocytic function. Thus, Aβ oligomers could induce neurobiological changes before plaque deposition.

Early symptoms of AD reach beyond memory loss, including sleep disturbance, psychosis, and social isolation [10]. Depressive symptoms are also common in the early stages and depression is a strong risk factor for AD. Whether depression is causative, or a prodromal indication is still a question of discussion [11]. Interestingly, antidepressant treatment such as ketamine or monoamine oxidase inhibitors has been shown to reduce cognitive deficits as well as pathology in AD [12, 13].

Recent imaging work suggests reduced synaptic density already at early stages of AD [14, 15] whereas clinical data show increased functional connectivity and synchronization of neuronal activity early in the disease [16]. These results appear contradictory, and we still need to better understand the functional changes of synaptic transmission in early AD. In this context, a deficit in neuronal activity set-point such as an imbalance between firing and neuronal plasticity, has been proposed to underlay early development of the pathology [17]. Interestingly, preclinical studies further emphasize the development of early synaptic deficits in AD, with demonstration of synaptic impairments at the pre-plaque stage in an *App* knock-in mouse model [18, 19] and impaired synaptic

plasticity in a hypercholesterolemia mouse model of AD [20].

Reactive astrocytes around plaques are very well described [21] and can be a consequence of Aβ accumulation [22]. More recently, astrocytic reactivity has been demonstrated at an early stage in the progression of AD [23, 24] and increased level of the glial fibrillary acidic protein (GFAP) has been detected in the cerebrospinal fluid of patients early in the disease [25]. Together with the fact that healthy astrocytes are important for Aβ clearance, thus reactive astrocytes could facilitate Aβ accumulation [26], these findings have led to the proposal of an astrocytic origin of the disease [27]. Early astrocyte reactivity in AD is compatible with synaptic changes due to the close interaction between astrocytic and synaptic function. Reactive astrocytes affect synapses through several mechanisms [28]. Among other things, reactive astrocytes have been shown to express monoamine oxidase type B (MAO-B) [29] resulting in *de novo* synthesis of GABA and an increased tonic inhibition of adjacent neurons [30].

Many animal models have been engineered in order to understand the mechanisms underlying AD, yet none of them recapitulate all the symptoms of the pathology [31]. One common feature in older models is an overproduction of the amyloid precursor protein, resulting in an important Aβ accumulation at a young age. The App^{NL-F} mouse line is a late onset knock-in model of AD that is useful to investigate early stages of the pathology. This model carries two disease causing mutations (the Swedish mutation, NL and the Beyreuther/Iberian mutation, F) in the endogenous *App* gene [32] and hence free from App overexpression. The App^{NL-F} mouse does not develop pathological plaques until 9 months of age [33]. While no tau pathology has been unveiled in this model [34], except increased phosphorylation of some sites [35], many molecular changes such as autophagy disturbances [36] and mitochondria dysfunctions [37] were reported both *in vivo* and *in vitro* [38]. Interestingly, early changes in the synapse structure and function has been identified in the cortex of 6-month-old App^{NL-F} animals [19, 39].

In the present study we used behavioral, electrophysiological and molecular readouts to understand early changes in this App^{NL-F} knock-in mouse model of AD. Our analysis revealed reduced synaptic activity and impaired synaptic plasticity associated to reactive-like astrocytes. These neuronal and astrocytic dysfunctions correlate with increased depressive-like behavior and could be partially cor-

rected by treatment with either the MAO-B inhibitor deprenyl or the fast-acting antidepressant ketamine.

MATERIAL AND METHODS

Animals

App^{NL-F} mice, model of AD, were bred locally at Uppsala University. These mice carry the Swedish (KM670/671NL) and the Beyreuther/Iberian (I716F) mutations in the App gene. Age-matched C57Bl6 mice were bought from Charles River (Germany). Both strains were housed in the same conditions, on a 12 : 12 light-dark cycle and with access to food and water *ad libitum*. All experiments were conducted in 6-month-old males, where increased insoluble Aβ was detected but where Aβ-plaques were absent (Supplementary Figure 1).

The study was conduct in accordance with the Declaration of Helsinki and was approved by the Swedish board of animal use (Jordbruksverket permit #5.2.18–03389/2020) and accepted by the ethics committee at Uppsala University (application DOUU 2020-022).

Drugs

Tetrodotoxin (TTX; Tocris 4368-28-9) was diluted in artificial cerebrospinal fluid (aCSF) and used in patch clamp experiments to measure mini excitatory post-synaptic currents (mEPSC), at a concentration of 1 μM.

NBQX (Tocris 1044), DL-AP5 (Tocris 3693), and Picrotoxin (PTX; Tocris 1128) were diluted in aCSF and used in patch clamp experiments to measure tonic GABA current, at a concentration of 10 μM, 50 μM, and 100 μM respectively.

(R)-(-)-Deprenyl hydrochloride (deprenyl; Tocris 1095) was diluted in aCSF and was used in the patch clamp and the field recording experiments, at a concentration of 100 μM.

Ketamine (Ketaminol® vet., 100 mg/kg, Intervet) was diluted in vehicle solution (natriumchloride, NaCl 0.9%) and delivered intraperitoneally (i.p.; 5 mg/kg) 24 h prior to experiments.

Behavioral analysis

Animals were habituated to the experimental room 20 min prior to experiments. The luminosity of the room was set on 30 lux and the temperature at 21°C ± 1°C. The tests were performed in the following order, with at least three days between each test.

Open field test

The animals were free to explore a spatial-cue-free square arena (50 cm × 50 cm) for 10 min. The central zone and peripheral zone were defined in the Ethovision software (Noldus tech, The Netherlands). The area of the central zone was defined as 50% of the area of the arena. The total travelled distance, the time spent in the central area, as well as the number of entries in the central zone, were automatically analyzed by the software.

Five-trials social memory test

The mice were habituated to an empty square arena (50 cm × 50 cm) for 10 min, followed by 5 min exploration of the same arena with an empty removable cage (8 cm × 8 cm × 9 cm). An unknown mouse (same genotype, same fur color, same age, and same gender as the test mouse) was placed for 5 min in the removable cage for four consecutive trials, separated by 10 min. One hour after the fourth trial, a new unknown mouse was placed in the cage for 5 min. Social interactions were manually scored.

Olfactory habituation/dishabituation test

The mice were isolated in individual standard cages in which they performed the whole experiment and habituated for at least 2 min. Cotton swabs soaked with non-social odors (melon and banana) or social odors (one from their homepage and one from a non-familiar cage) were presented to the animal for 2 min. Each odor was presented three times.

Elevated plus maze

The maze was composed of two open arms, two closed arms, linked together at a central platform and positioned 50 cm above ground. Mice were placed on the central platform facing one open arm and were let to explore for 5 min. The number of entries and the time spent in the open arms were manually scored. An animal was considered "in the arm" when the four paws crossed the virtual line between the central platform and the considered arm.

Forced swim test

The mice were placed in a cylinder (30 cm high, φ 18 cm) filled with 25 ± 1°C water to a height of 17 cm where no part of the animal could touch the

bottom. The mice were left in the cylinder for 6 min, and the time spend immobile was quantified during the last 4 min. Latency to first immobility and the total time of immobility were manually scored. An animal was considered as immobile when it was floating and none of the paws nor the tail was moving.

Emotionality z-score

Z-normalization was used in this study as a complementary measurement for emotionality-related behavior, obtain from different paradigms [40]. Raw behavioral data (parameters of interest) were normalized to the control group using the following equation $z = (X - \mu)/\sigma$ with X being the individual value for the considered parameter, μ being the mean of the control group and σ being the standard deviation of the control group. Each parameter of interest gave a parameter z-score (zSC_param), adjusted so that an increased score reflects an increased emotionality. For each test, all parameter scores were averaged into a test score (zSC_test), and eventually averaged to give an individual emotionality z-score.

More details about the exact list of parameters of interest and the mathematical method are available in Supplementary Tables 1 and 2.

Electrophysiology

Brain slicing

For the preparation of acute slices, mice were anesthetized with isofluorane and decapitated soon after the disappearance of corneal reflexes. 300 μm thick horizontal sections were prepared using a Leica VT1200 vibrating microtome (Leica Microsystems, Nussloch, Germany) in dissection solution containing 250 mM sucrose, 2.5 μM KCl, 1.4 mM NaH$_2$PO$_4$, 26 mM NaHCO$_3$, 10 mM glucose, 1 mM CaCl$_2$ and 4 mM MgCl$_2$, and bubbled with carbogen gas (5% CO$_2$, 95% O$_2$). Hippocampi were dissected and slices were placed in a recovery chamber filled with aCSF containing (in mM): 130 NaCl, 3.5 KCl, 1.25 NaH$_2$PO$_4$, 24 NaHCO$_3$, 10 glucose, 2 CaCl$_2$ and 1.3 MgCl$_2$ and bubbled with carbogen gas.

Patch clamp recording

After a recovery period of at least 2 h, slices were transferred in a submerged recording chamber with a perfusion rate of 2–3 mL per min with standard aCSF, tempered at $32 \pm 1°C$ and bubbled with carbogen gas. Borosilicate glass pipettes with a tip

resistance of 4–5 MΩ were used for patching neurons. The glass pipettes were filled with a solution containing (in mM) 110 K-gluconate, 10 KCl, 4 Mg-ATP, 10 Na$_2$-phosphocreatine, 0.3 Na-GTP, 10 4-(2-hydroxyethyl)piperzine-1-ethanesulfonic acid (HEPES) and 0.2 ethylene glycol tetraacetic acid (EGTA) (pH 7.2–7.4; 270–290 mOsm). Glutamatergic neurons were identified by shape and patched at the border between stratum pyramidale and stratum radiatum in area CA1 of the hippocampus. Spontaneous excitatory post-synaptic currents (sEPSC) were recorded in absence of any drugs, whereas mEPSC were recorded in the presence of 1 μM TTX. To block the monoamine oxidase B (MAO-B), deprenyl (100 μM) was added in the recovery chamber and all the recording were done under tonic deprenyl treatment.

The access resistance was monitored throughout the recordings and data were included only for stable values (<30% variation). The signal was acquired using an Ag/AgCl electrode connected to a Multiclamp 700B amplifier, digitized with Digidata 1440A and handled with the Clampex software (v. 10.0; Molecular Devices). Traces were analyzed using the Easy electrophysiology software (v. 2.4). The event detection was based on a template fitting method. Probe recordings (three recordings of 1 min each) from C57Bl6 wild type acute hippocampus slices were used to generate and refine a template from representative events corresponding to an average of ten to twenty detected EPSC. Event detection in App^{NL-F} and C57Bl6 controls acute slices was then run on a semi-automatic method: each event detected fits the previously generated template. A minimum amplitude threshold of 10 pA was applied: all events that were detected between 0 pA and 10 pA were discarded. Each recording was analyzed on a period of 1 min.

GABA currents [41, 42] were recorded in the presence of NBQX (10 μM) and DL-AP5 (50 μM). After recording a stable baseline, picrotoxin (PTX; 100 μM) was added to block GABA$_A$ receptors. Tonic GABA current was calculated as the difference in mean holding current for 1 min after achieving a stable shift in baseline with PTX compared to before PTX.

Field recording

After a recovery period of at least 2 h, slices were transferred in a submerged recording chamber with a perfusion rate of 2–3 ml per minute with either stan-

dard aCSF or deprenyl (100 μM)-containing aCSF, tempered at $32 \pm 1°C$ and bubbled with carbogen gas. An extracellular borosilicate recording pipette filled with aCSF was placed in the stratum radiatum of area CA1 and field excitatory post-synaptic potentials (fEPSP) were evoked by electrical stimulation of the Schaffer collaterals using a bipolar concentric electrode (FHC Inc., Bowdoin, ME), connected to an isolated stimulator (Digitimer Ltd., Welwyn Garden City, UK). Recordings were performed with the stimulus intensity to elicit 30–40% of the maximal response and individual synaptic responses were evoked at 0.05 Hz (every 20 s). The acquired signal was amplified and filtered at 2 kHz (low-pass filter) using an extracellular amplifier (EXT-02F, NPI Electronic, Tamm, Germany). Data were collected and analyzed using a Digidata 1440A, Axoscope and Clampfit softwares (Molecular Devices, San Jose, CA). Responses were quantified by determining the slope of the linear rising phase of the fEPSP (from 10% to 70% of the peak amplitude). The response was normalized to the average baseline measured in the last 10 min prior to the start of the experiment.

To study long term synaptic plasticity, we used ten theta-bursts separated with 200 ms. Each theta-burst is four pulses at 100 Hz, a stimulation protocol tested not to be enough to trigger long term potentiation (LTP) in slices from C57Bl6 mice.

Immunohistochemistry

Perfusion and brain extraction

Mice were deeply anesthetized with a mixture of ketamine (100 mg/kg) and xylazine (16 mg/kg) i.p. In absence of corneal reflexes, mice were transcardially perfused with NaCl 0.9% followed by a 4% PFA solution. The brain was extracted and post-fixed in a 4% PFA solution for 48 h, washed in PBS for 24 h and placed in a 30% sucrose + 1% natrium azide solution until further use.

Slicing and staining

Brains were cut in a cryostat at 140 μm thick sections (for astrocytic morphology analysis) and 40 μm (for inflammation markers analysis). For GFAP staining, free-floating slices were treated with a peroxide solution (10% methanol and 10% H_2O_2 in PBS) for 20 min followed by antigen retrieval solution (Tris 10 mM EDTA, 10% Tween-20) at 80°C. After blocking steps with normal donkey serum, slices were incubated with primary glial fibrillary acidic protein (GFAP, Synaptic system 173–004; 1 : 500) and primary connexin 43 (Cx43, Invitrogen 71-0700; 1 : 500) for 72 h (for the morphology analysis); 40 μm thick slices were incubated with vimentin primary antibody (Merk, AB5733) for 48 h. Slices were incubated with the appropriate secondary antibodies for 2 h, DAPI (1 : 5000) was added to counterstain nuclei. Slices were then mounted on non-coated microscope glass coverslips using the fluoromount mounting medium (Invitrogen, 00-4958-02). Two z-stacks (0.25 μm step size) per slice (two slices per animal), were obtained from the CA1 region of the hippocampus using a confocal microscope (Zeiss LSM700) with a 63× oil objective.

Image analysis

For morphological analysis, the z-stacks were deconvoluted using the Hyugens software (Scientific Volume Imaging) and noise-saturated pixels were removed. GFAP/DAPI images were segmented thanks to a pixel classification protocol using the Ilastik software [43]. Using Image J (NIH), centroids of the nuclei were determined, DAPI/GFAP images were merged and each astrocyte were manually separated from the astrocytic syncytium thanks to the Cx43 staining giving the precise location of each connexon. Every astrocyte touching at least one border of the z-stack was automatically removed in order to exclude truncated astrocytes. The center of the sholl analysis was defined by the centroid of the nuclei. Branch counting started at a radius of 7 μm and ended at 45 μm from the center, with a step size of 2 μm. Subsequent data (i.e., sholl analysis and volume occupied by the cell) were automatically generated thanks to the Image J software using a custom macro. Detailed workflow is available in the Supplementary Figure 2.

For the vimentin signal analysis, maximal intensity projections images where thresholded and cells expressing vimentin were identified and analyzed automatically in the ImageJ software. A size filter was applied to exclude vessels. The total vimentin staining in all detected regions of interest was summed for each image.

Statistical analysis

IBM SPSS Statistics (v. 28 IBM corp) was used to perform the statistical analysis. For each measured variable, a Shapiro-Wilk test for normality and Levene's test for homogeneity of variances were con-
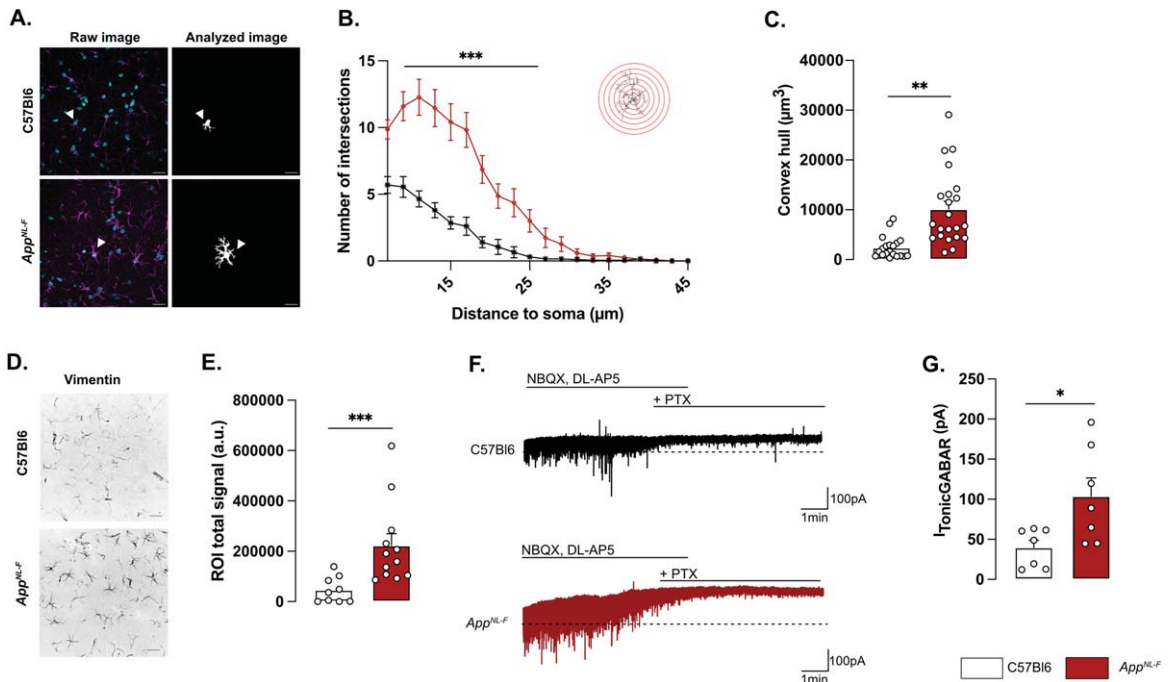
Fig. 1. **Reactive-like astrocytes in 6-month-old App^{NL-F} mice.** Confocal z-stack images of immunohistochemical labelled GFAP-positive astrocytes in area CA1 of the hippocampus were used to analyze astrocytes morphology. Magenta: GFAP, cyan: DAPI (A, left panel). Images were deconvoluted and astrocytes were segmented and isolated based on connexin staining. Representative of analyzed image are displayed in A, right panel. White arrows show a representative astrocyte. Scale bar for both view: 20 μm. Sholl analysis revealed an increased number of intersections from 7 to 25 μm from the soma (B) Mann-Whitney test: ***$p < 0.001$ significant from C57Bl6. The average volume occupied by the astrocyte (C) was also increased in App^{NL-F} compared to C57Bl6 mice (Mann-Whitney test: **$p < 0.01$ significantly different as shown). For all measurements, C57Bl6: $n = 20$ cells in three animals, App^{NL-F}: $n = 22$ cells in three animals. Quantification of the vimentin positive signal (D) revealed an increased signal in App^{NL-F} mice compared to C57Bl6 animals (Mann-Whitney test: ***$p < 0.001$). E depicts representative vimentin signal for both genotypes. Scale bar: 20 μm. C57Bl6: $n = 9$ images from 3 mice. App^{NL-F}: $n = 12$ images form 4 mice. Tonic GABA currents were recorded in pyramidal cells in the presence of NBQX and DL-AP5. Representative traces with baseline before blocking GABA is shown as a dashed line (E). Average tonic GABA currents are significantly higher in App^{NL-F} mice compared to C57Bl6 (F) Mann-Whitney test: *$p < 0.05$ significantly different as shown. C57Bl6: $n = 7$ cells recorded in five animals; App^{NL-F}: $n = 7$ cells recorded in four animals.

ducted. If none of them was significant (indicating a normal distribution and homogeneous variances), a student *t*-test was conducted. If one or the other was significant, a Mann-Whitney test was conducted. Because of the experimental design, and the presence of multiple variables measured at once, a two-way ANOVA followed, if applicable, by a Bonferroni correction was used to analyze the ELISA (see Supplementary Material) and the astrocytic morphology experiments. A one-way ANOVA followed, if applicable, by a Bonferroni correction was used for the five-trials social memory test and the olfactory habituation/dishabituation test. For all the tests, 0.05 was set as the significance threshold. All results are shown as mean ± S.E.M. and the individual values are displayed on each graph. The number of animals used, the number of slices and the number of recorded cells is described in each figure caption.

RESULTS

Astrocytes display reactive-like phenotype in 6-month-old App^{NL-F} mice

Morphologically, reactive astrocytes are characterized by a swollen soma and increased branching. Morphology analysis of GFAP stained astrocytes in brain sections from 6-month-old mice revealed a reactive-like morphology in App^{NL-F} mice compared to C57Bl6 mice (Fig. 1A–C). The morphological complexity was quantified as an increased number of branches, counted every 2 μm from the soma (Two-way ANOVA with distance and genotype as the main factors. Distance: $F_{(8,230)} = 98.167$, $p < 0.001$; Genotype: $F_{(1,40)} = 26.845$; $p < 0.001$; Interaction: $F_{(8,230)} = 19.927$, $p < 0.001$). The difference was particularly prominent between 7

and 25 μm from the soma (Fig. 1B). Moreover, the volume occupied by each astrocyte was bigger in App^{NL-F} mice compared to C57Bl6 mice (C57Bl6: 2396 ± 486.1 μm^3 versus App^{NL-F}: 10133 ± 1568 μm^3, $p < 0.01$; Fig. 1C). The number of astrocytes (GFAP-positive cells) was not significantly different in App^{NL-F} compared to C57Bl6 controls (Supplementary Figure 2D) when estimated as the number of astrocytes per image. Astrocytic reactivity is not limited to morphological changes, and we further analyzed the commonly used astrocytic reactivity marker vimentin. The analysis in the hippocampus revealed a significant increased vimentin signal in App^{NL-F} mice compared to C57Bl6 controls (46218 ± 17227 a.u. versus 222674 ± 46862 a.u, $p < 0.001$; Fig. 1D, E).

Reactive astrocytes have been shown to synthesize and release GABA [30] and we thus recorded tonic GABA currents in pyramidal neurons in area CA1 (Fig. 1F). Indeed, tonic GABA currents were significantly higher in App^{NL-F} mice compared to C57Bl6 (103.8 ± 22.63 pA versus 39.83 ± 9.057 pA, $p < 0.05$; Fig. 1G).

Impaired synaptic transmission and plasticity in App^{NL-F} mice

Whole-cell patch clamp recordings from pyramidal neurons of area CA1 showed that resting membrane potential was significantly depolarized in App^{NL-F} mice compared to C57Bl6 mice (Fig. 2A; –51.74 ± 1.32 mV versus –56.18 ± 1.38 mV; $p < 0.05$). Spontaneous synaptic activity in active hippocampal network (sEPSC) was not different between the two strains in neither frequency amplitude, decay or rise time of sEPSC (Fig. 3A-D). However, when action potentials were blocked with the sodium channel blocker TTX (1 μM) to record spontaneous release of individual synaptic vesicles (mEPSC), a reduced frequency of the mEPSC (Fig. 2B) was observed in App^{NL-F} mice compared to C57Bl6 mice (0.27 ± 0.04 Hz versus 0.56 ± 0.08 Hz; $p < 0.01$), whereas the amplitude of mEPSCs remained unchanged (C57Bl6: –21.71 ± 1.48 pA, App^{NL-F}: –19.65 ± 1.43 pA, Fig. 2C). There were no differences in the decay or rise time of mEPSC (Supplementary Figure 3E, F respectively).

Changes in basic synaptic transmission can entail changes in synaptic plasticity, previously described as synaptic mistuning [44]. To investigate the state of plasticity in App^{NL-F}, the possibility to undergo

long-term potentiation (LTP) was examined, using a subthreshold stimulation protocol that did not evoke LTP in C57Bl6 mice. Ten theta-bursts stimulation of Schaffer collaterals induced an immediate potentiation of synaptic strength, as measured as the increased slope of the evoked fEPSP, in both genotypes ($p < 0.001$; Fig. 2D, E). However, 1 h after stimulation, the fEPSP had progressively returned to baseline in control animals, whereas the magnitude of the fEPSP was still significantly increased in App^{NL-F} mice ($p < 0.001$ different from the baseline; Fig. 2D, F). Thus, already at 6 months, App^{NL-F} mice have changes in synaptic function, detected as reduced frequency of synaptic events and a reduced threshold for potentiation.

MAO-B blocking restores synaptic transmission and plasticity in App^{NL-F} mice

To examine the relationship between tonic GABA and synaptic function, the astrocytic GABA-synthesizing enzyme MAO-B was blocked by pre-incubating the slices with deprenyl (100 μM). Blocking MAO-B caused an increase in the resting membrane potential in deprenyl treated slices from App^{NL-F} mice compared to non-treated slices (–54.84 ± 1.994 mV versus –46.30 ± 3.251 mV, $p < 0.05$, Fig. 3A). Moreover, deprenyl increased the frequency of mEPSC events from 0.05 ± 0.008 Hz, in non-treated slices to 0.26 ± 0.03 Hz in deprenyl treated slices ($p < 0.01$, Fig. 3B) and the amplitude from –15.23 ± 2.10 pA to –23.06 ± 1.79 pA ($p < 0.05$, Fig. 3C). For spontaneously evoked synaptic events, deprenyl treatment significantly increased the amplitude of sEPSC but not the frequency (Supplementary Figure 3G, H). Deprenyl did not affect rise time nor decay time of either sEPSC or mEPSC (Supplementary Figure 3I-L).

Pre-treatment with deprenyl also had an effect on synaptic plasticity. Unexpectedly, synaptic potentiation was reduced in slices from App^{NL-F} mice that had been pretreated with deprenyl compared to non-treated slices (Fig. 3D). Deprenyl reduced fEPSP magnitude both at 1–5 min (App^{NL-F} + aCSF: 1.70 ± 0.05, App^{NL-F} + deprenyl: 1.51 ± 0.03) and 55–60 min (App^{NL-F} + aCSF: 1.519 ± 0.07, App^{NL-F} + deprenyl: 1.23 ± 0.04) after the same sub-threshold stimulation as used above (Fig. 3E, F).

Taken together, our results show that already at a pre-plaque stage App^{NL-F} mice have reactive-like astrocytes. We further suggest that GABA release from astrocytes contribute to synaptic impairment
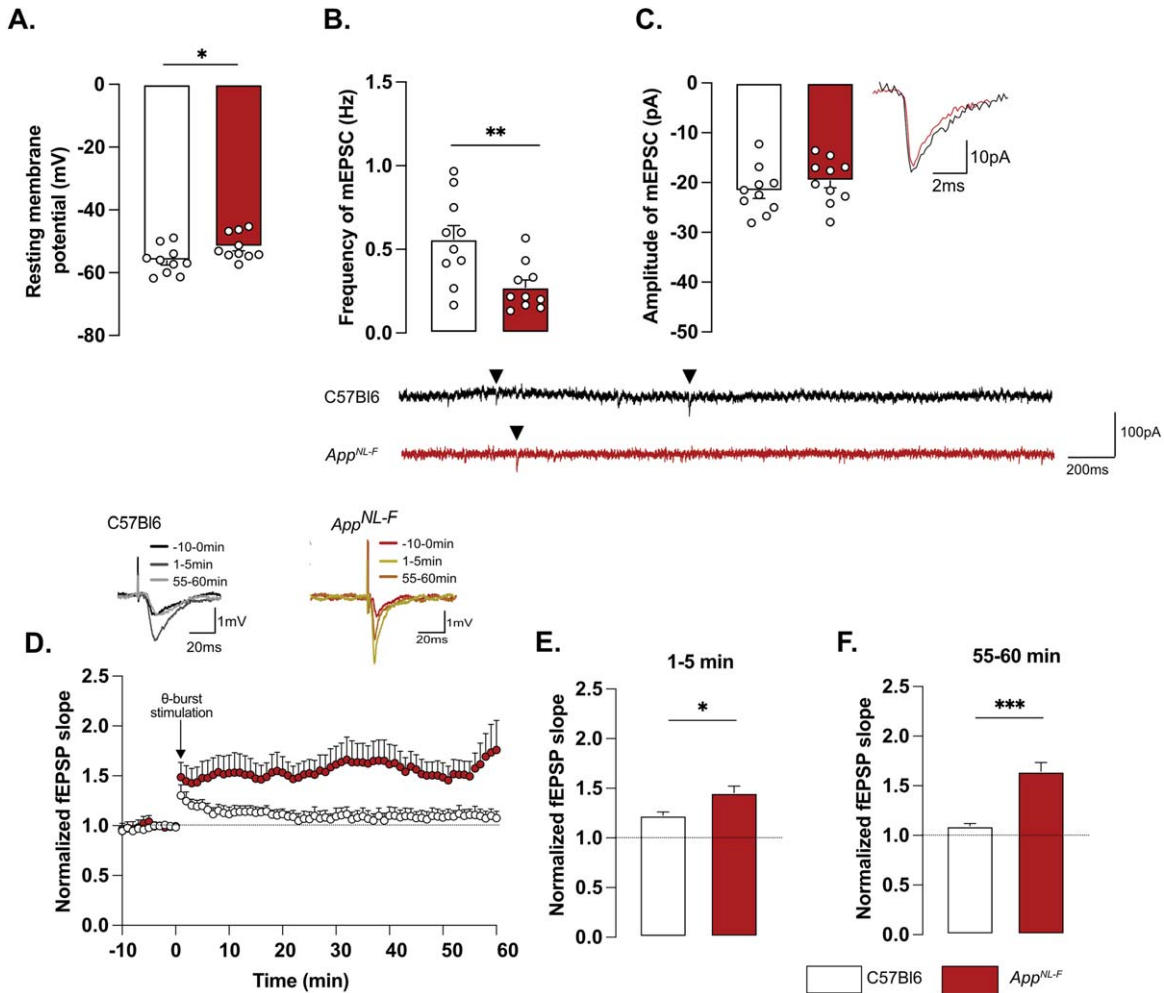
Fig. 2. **Mistuned synapses in 6-month-old App^{NL-F} mice.** Average resting membrane potential of pyramidal neurons of area CA1 of the hippocampus is significantly higher in App^{NL-F} mice compared to C57Bl6 mice (A). Recordings of mEPSC in the same cells show reduced frequency of events (B) in App^{NL-F} compared to C57Bl6 mice, with no changes in amplitude (C). Representative traces for mEPSC are shown under graphs. Student t-test, **$p < 0.01$ statistically significant as shown. For all variables, C57Bl6: $n = 10$ cells recorded in seven animals, App^{NL-F}: $n = 10$ cells recorded in seven animals. fEPSP were recorded after Schaffer collaterals stimulation in the area CA3. We recorded the response of post-synaptic neurons in area CA1. A subthreshold *theta*-burst (θ-burst) stimulation was applied and fEPSP magnitude was monitored for 1 h. The fEPSP slope was normalized to the average baseline value and displayed as the average per minute (D). Representative traces are shown on top. The θ-burst induced a significant potentiation in both App^{NL-F} and C57Bl6 mice at 0–5 min after stimulation (E). However, at 55–60 min, the fEPSP magnitude is almost back to baseline in C57Bl6 mice and is significantly increased in App^{NL-F} mice (F). Student t-test: *$p < 0.05$, ***$p < 0.001$ statistically significant as shown. C57Bl6: $n = 6$ recordings in three animals, App^{NL-F}: $n = 9$ recordings in five animals.

since in the hippocampus, MAO-B is predominantly expressed by reactive astrocytes [45]. A neuronal origin of tonic GABA is however not explicitly ruled out.

App^{NL-F} mice show a lack of motivation and a mild depressive-like behavior

Deficits in plasticity is typically linked to memory problems. However, despite deficits in plasticity at 6 months, App^{NL-F} mice have no spatial memory impairment at this age [46]. Other forms of memory have not been explored, prompting us to investigate the possible effect on social memory. In the five-trials social memory test the social interactions with an unknown animal in four consecutive trials is used to evaluate social memory whereas the interaction with a new animal on the fifth trial is used to assess the social novelty preference and motivation [47, 48] (Fig. 4A). A similar decrease
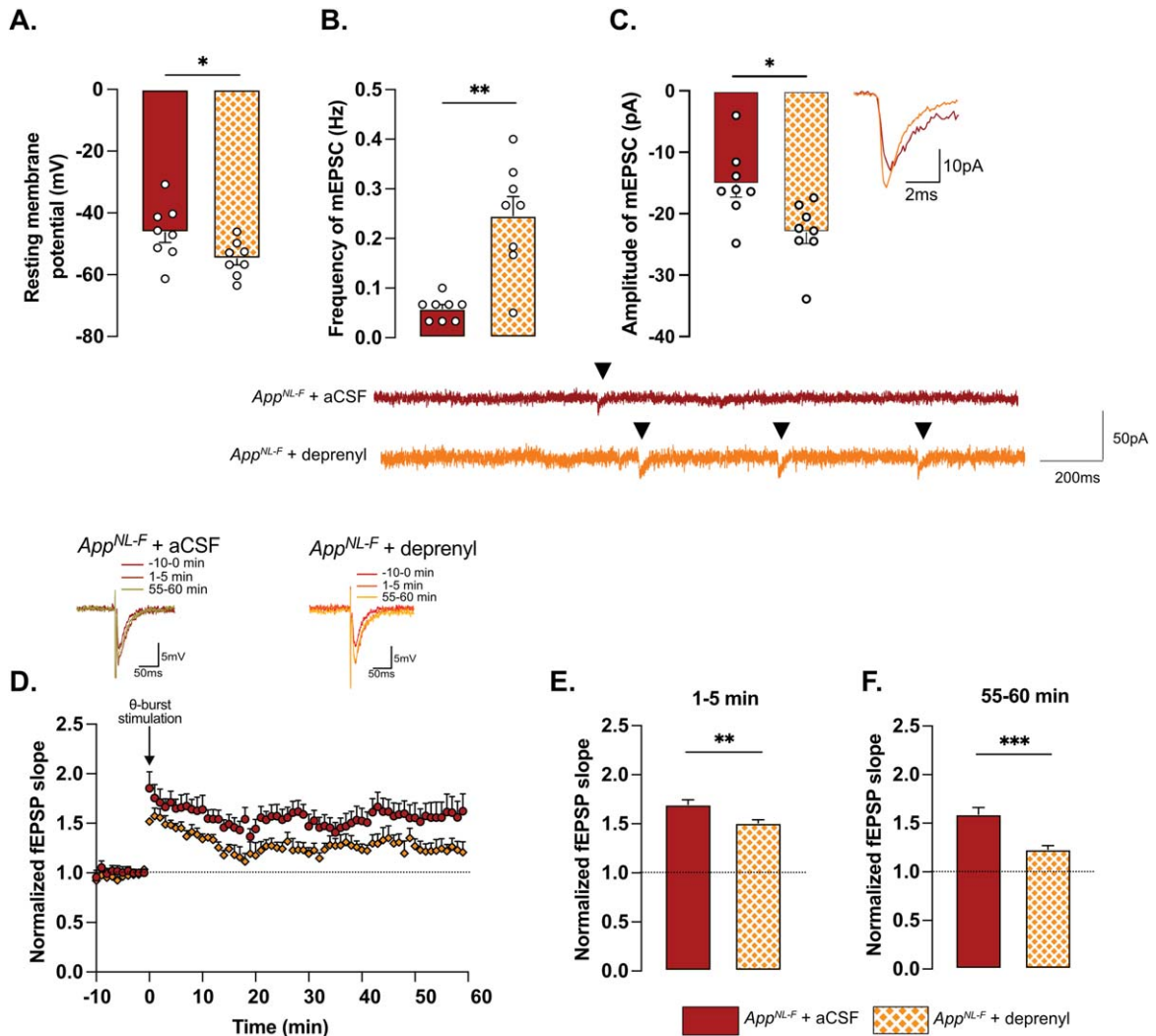
Fig. 3. **Retuned synapses after MAO-B blocking by deprenyl in 6-month-old App^{NL-F} mice.** Pre-treatment of hippocampal slices with the MAO-B blocker deprenyl significantly decreases resting membrane potential in pyramidal cells in App^{NL-F} mice (A). Blocking MAO-B increased both frequency (B) and amplitude (C) of mEPSC. Representative traces are shown under graphs. Student *t*-test and Mann-Whitney test: **$p < 0.01$; ***$p < 0.001$ statistically significant as shown. App^{NL-F} + aCSF: $n = 8$ cells recorded in four animals; App^{NL-F} + deprenyl: $n = 8$ cells recorded in four animals. The subthreshold theta-burst (θ-burst) stimulation induced long term potentiation in both treated and untreated slices from App^{NL-F} mice (D). Representative traces are shown on top. When we compared the average fEPSP magnitude at 0–5 min and 55–60 min after stimulation, the potentiation was significantly lower after deprenyl pre-treatment (E, F). Mann-Whitney test: **$p < 0.01$, ***$p < 0.001$ statistically significant as shown. App^{NL-F} + aCSF: $n = 6$ recordings in four animals, App^{NL-F} + deprenyl: $n = 5$ recordings in three animals.

in social interactions was observed over the four first trials in both App^{NL-F} and C57Bl6 animals (Fig. 4B), suggesting no social memory impairments at 6 months of age. However, on the fifth trial the social interactions with a new animal were increased in control mice (8.93 ± 2.98 s on trial 4 versus 28.41 ± 2.98 s on trial 5; $p < 0.05$) whereas no change was observed in the fifth trial compared to the fourth in App^{NL-F} mice (10.74 ± 1.95 s

on trial 4 versus 12.92 ± 4.19 s on trial 5). The latency to first interaction was similar in both groups during the first trial, (C57Bl6: 26.32 ± 13.31 s, App^{NL-F}: 11.69 ± 6.903 s); however, it was significantly increased in App^{NL-F} mice compared to C57Bl6 mice on the fifth trial (132.01 ± 41.24 s versus 9.73 ± 5.13 s; $p < 0.01$; Fig. 4C). Together, these results show an intact social memory in App^{NL-F} mice at 6 months, and suggest a slight reduced
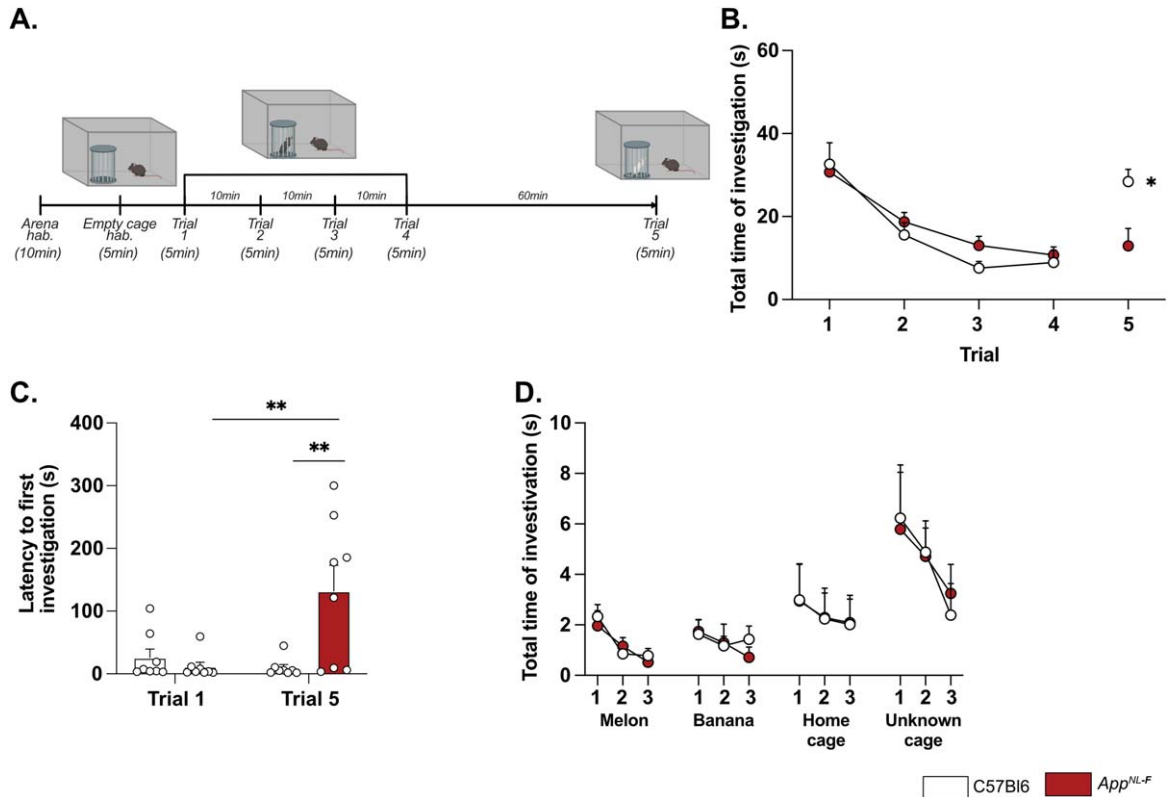
Fig. 4. App^{NL-F} **mice shown no social memory impairments but a lack of motivation.** In the five-trials social memory test (A), App^{NL-F} mice show no memory deficits as seen by the progressive decrease in social interactions over four consecutive trials (B). On the fifth trial, when a new animal is presented, C57Bl6 mice regain interest and the time of interaction is increased, whereas the time of interaction is not different in the fifth trial versus the fourth one in App^{NL-F} mice. Two-way ANOVA for repeated measured with the genotype and the trial as the main factors. Bonferroni multiple comparison $*p < 0.05$ statistically different trial 4 versus trial 5. Latency to first investigation (C) is similar between genotypes in the first trial. However, it is significantly increased in App^{NL-F} on the fifth trial compared to C57Bl6 and to App^{NL-F} in trial 1. Two-way ANOVA for repeated measured with the genotype and the trial as the main factors. Bonferroni multiple comparison; Bonferroni multiple comparison: $**p < 0.01$: statistically different as shown. C57Bl6: $n = 8$, App^{NL-F}: $n = 8$. In the olfactory habituation/dishabituation test (D), we presented four different odors for three times 2 min each. The time of interaction with the probe was similar in C57Bl6 and App^{NL-F} at all timepoints and for all odors. C57Bl6: $n = 9$, App^{NL-F}: $n = 10$.

preference for social novelty, evident at the fifth trial. To rule out potential olfactory dysfunctions, which could interfere with the social memory tests, we performed an olfactory habituation/dishabituation test [49] (Fig. 4D). Four odors were tested and no significant differences between odor recognition was observed between C57Bl6 and App^{NL-F} mice. Both strains spent more times interacting with social odors, especially from an unknown cage, showing the absence of olfactory problem as well as a capacity of App^{NL-F} mice to discriminate between social and non-social odors. Furthermore, since motor coordination could be a confounding factor in behavior tests, motor coordination was evaluated on the rotarod. No difference between C57Bl6 and App^{NL-F} mice was observed in the performance in the rotarod (Supplementary Figure 4).

A reduced preference for social novelty in 6-month-old App^{NL-F} mice is consistent with clinical studies on patients with AD [50] and prompted further research of emotional symptoms. In the open field test App^{NL-F} animals had a significant reduction of the travelled distance compared to C57Bl6 (3543 ± 61.1 cm versus 5663 ± 421.1 cm; $p < 0.001$; Fig. 5A). The number of entries in the central area was significantly lower in the App^{NL-F} mice compared to C57Bl6 mice. (6.50 ± 1 entries versus 30.75 ± 4 entries; $p < 0.01$; Fig. 5B) whereas the time spent in the central zone was not significantly different (C57Bl6: 81.16 ± 6.23 s, App^{NL-F}: 82.30 ± 7.22 s; Fig. 5C). In the elevated plus maze the number of entries in the open arms (anxiogenic area) was significantly reduced in App^{NL-F} mice compared to C57Bl6 (3.25 ± 1 entries versus 6.12 ± 1
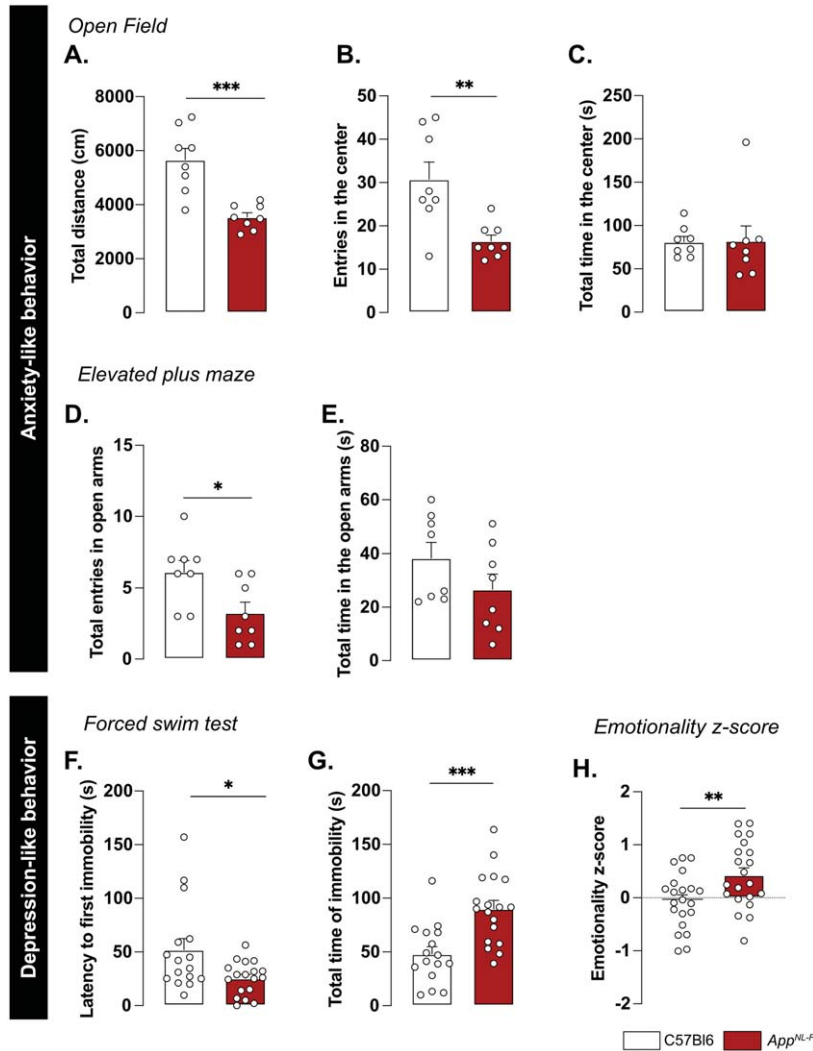
Fig. 5. App^{NL-F} **mice display mild depressive-like behavior.** In the open field test, the total travelled distance (A) is reduced in App^{NL-F} compared to C57Bl6, as well as the number of entries in the central area (B). The total time in the open area is not different between the two strains (C). Mann-Whitney test: **$p < 0.01$, ***$p < 0.001$ statistically different as shown. C57Bl6: $n = 8$, App^{NL-F}: n = 8. In the elevated plus maze, the number of entries in the open arms is significantly lower in App^{NL-F} compared to C57Bl6 (D) whereas the total time spent in the open arms (E) remains unchanged between genotypes. Student *t*-test: *$p < 0.05$ statistically different as shown. C57Bl6: $n = 8$, App^{NL-F}: $n = 8$. In the forced swim test, the latency to first immobility is lower in App^{NL-F} mice compared to C57Bl6 (F), while the total time of immobility is higher (G). Mann-Whitney and student *t*-test: *$p < 0.05$, ***$p < 0.001$ statistically different as shown. C57Bl6: $n = 16$, App^{NL-F}: $n = 18$. The emotionality z-score is an integrative score allowing comparison of multiple factors, calculated on different scales and includes parameters from the different behavioral tests described above (see supplementary information). The emotionality z-score is significantly higher in App^{NL-F} mice compared to C57BL6 (H). Student *t*-test: **$p < 0.01$ statistically significant as shown. C57Bl6: $n = 21$, App^{NL-F}: $n = 21$.

entries; $p < 0.05$; Fig. 5D) whereas the total time spent in this area was not different between the strains (C57Bl6 : 38.38 ± 5.68 s, App^{NL-F}: 26.63 ± 5.76 s; Fig. 5E).

We then explored the depression-like behavior in three different paradigms. In the forced swim test, the immobility was used as an indicator of helplessness. The latency to the first immobil-

ity was significantly reduced in App^{NL-F} mice (C57Bl6 : 52.05 ± 0.30 s, App^{NL-F}: 25.43 ± 3.70 s, $p < 0.05$; Fig. 5F) whereas the total time of immobility was significantly increased (C57Bl6 : 48.07 ± 6.89 s, App^{NL-F}: 90.07 ± 7.79 s; $p < 0.001$; Fig. 5G). In the splash test (see Supplementary Material), the lack of grooming reflects a lack of self-care. No significant differences in the grooming behavior were observed

in the App^{NL-F} mice compared to C57Bl6 (Supplementary Figure 4C-E). The sucrose preference test (supplementary methods), where a lack of preference for sugar compared to water is considered to reflect anhedonia, revealed no difference between the two strains (Supplementary Figure 4F).

These behavioral data suggest a slight anxiety- and depression-like behavior and this was quantified as an emotionality z-score [40]. We used several parameters per test to establish a z-score for each test (ZSc_test; Supplementary Table 1) and each ZSc_test was then combined into an emotionality z-score (Fig. 5H). The C57Bl6 mice were used as the control group and have an average z-score of zero (-0.05 ± 0.11). The App^{NL-F} mice had a significantly increased z-score (0.42 ± 0.13, $p < 0.01$) confirming depressive-like behavior in the 6-month-old App^{NL-F} mice.

A single dose of ketamine (5 g/kg) partially corrects depressive-like behavior in App^{NL-F} mice

A low dose of ketamine has antidepressant effects, and can also revert dysfunction in synaptic tuning [44]. Thus, an i.p. injection of either ketamine (5 mg/kg) or vehicle solution (NaCl 0.9%) was administered to 6-month-old App^{NL-F} mice and behavior was tested 24 h after injection. In the five-trials social memory test, ketamine did not affect social memory as shown by a similar decrease of social interaction over four consecutive trials, in both treatment conditions (Fig. 6A). As in our previous experiments, the social interaction measured in the fifth trial was not significantly different from the fourth trial in the vehicle treated animals (trial $4 : 18.90 \pm 4.66\%$ versus trial $5 : 38.20 \pm 5.91\%$, Fig. 6B). Ketamine did not have a significant effect on the social interaction on the fifth trial (trial $4 : 22.085 \pm 4.97\%$ versus trial $5 : 40.12 \pm 9.48\%$).

We further explored the antidepressant action of a single injection of 5 mg/kg ketamine. In the open field, none of the parameters total distance travelled (NaCl: 4331 ± 190.5 cm, ketamine: 4454 ± 229.3 cm; Fig. 6C), the number of entries in the center (NaCl: 20.19 ± 2.30 entries, ketamine: 22.69 ± 2.55 entries; Fig. 6D) and total time spent in that zone (NaCl: 66.11 ± 6.35 s, ketamine: 83.13 ± 10.32 s; Fig. 6E) were changed by the ketamine treatment. Likewise, ketamine had no effect on the number of entries in the open arms in the elevated plus maze (NaCl: 0.87 ± 0.40 entries, ketamine: 1.25 ± 0.25 entries; Fig. 6F) nor the total time spent in that zone (NaCl: 8.41 ± 3.2 s, ketamine: 1.12 ± 4.79 s; Fig. 6G).

In the forced swim test, no changes were observed in the latency to first immobility (NaCl: 20 ± 3.32 s, ketamine: 29.75 ± 6.56 s; Fig. 6H). However, there was a reduced total time of immobility in ketamine treated mice compared to NaCl treated (NaCl: 114.4 ± 2.02 s, ketamine: 71.88 ± 10.61, $p < 0.05$; Fig. 6I). Similarly, in the splash test, a reduced latency to first grooming (NaCl: 32.52 ± 3.71 s, ketamine: 16.30 ± 2.56 s, $p < 0.01$; Supplementary Figure 4G), increased frequency of grooming (NaCl: 7 ± 0.27, ketamine: 9.13 ± 0.69, $p < 0.05$; Supplementary Figure 4H) and an increased total time of grooming (NaCl: 145.7 ± 6.01 s, ketamine: 188.8 ± 3.56 s, $p < 0.05$; Supplementary Figure 4I) were observed after ketamine treatment.

The behavioral data was integrated into the emotional z-score (Fig. 6J) to assess the overall effect of ketamine on the depressive-like behavior of App^{NL-F}. Animals who received the vehicle solution were used as the control group with an average emotionality z-score of zero. No statistical difference was shown in the z-score between the two different groups. Thus, ketamine did not reverse all emotional symptoms in the App^{NL-F} mice. However, in line with the well-known antidepressant effect of ketamine [51], we show an effect of ketamine

Fig. 6. **Ketamine (5 mg/kg) partially restores emotionality in 6-month-old App^{NL-F} mice.** As previously shown, App^{NL-F} mice do not have social memory impairments, as the social interaction progressively declines over four trials. This learning curve is not affected by injections of NaCl of Ketamine 24 h before testing (A). Moreover, ketamine does not significantly affect the lack of motivation (B). App^{NL-F} + NaCl: $n = 16$, App^{NL-F} + ketamine: $n = 13$. In the open field test, neither the total travelled distance (C), the number of entries in the open area (D) nor the total time in that zone (E) is affected by ketamine. App^{NL-F} + NaCl: $n = 16$, App^{NL-F} + ketamine: $n = 13$. A similar profile was obtained in the elevated plus maze in which neither the number of entries in the open arms (F) or the total time in that zone (G) are affected. App^{NL-F} + NaCl: $n = 8$, App^{NL-F} + ketamine: $n = 8$. In the forced swim test, the latency to first immobility (H) is unchanged after ketamine treatment while the total time of immobility (I) is reduced. Student t-test: $^*p < 0.05$ statistically different as shown. App^{NL-F} + NaCl: $n = 8$, App^{NL-F} + ketamine: $n = 8$. Interestingly, the emotionality z-score (J) remains unchanged after ketamine 5 mg/kg treatment. App^{NL-F} + NaCl (left); $n = 16$, App^{NL-F} + ketamine (right); $n = 16$.

Five-trials social memory test

A.

B.

Open Field

C.

D.

E.

Elevated plus maze

F.

G.

Forced swim test

H.

I.

Emotionality z-score

J.

Social memory / Motivation

Anxiety-like behavior

Depression-like behavior

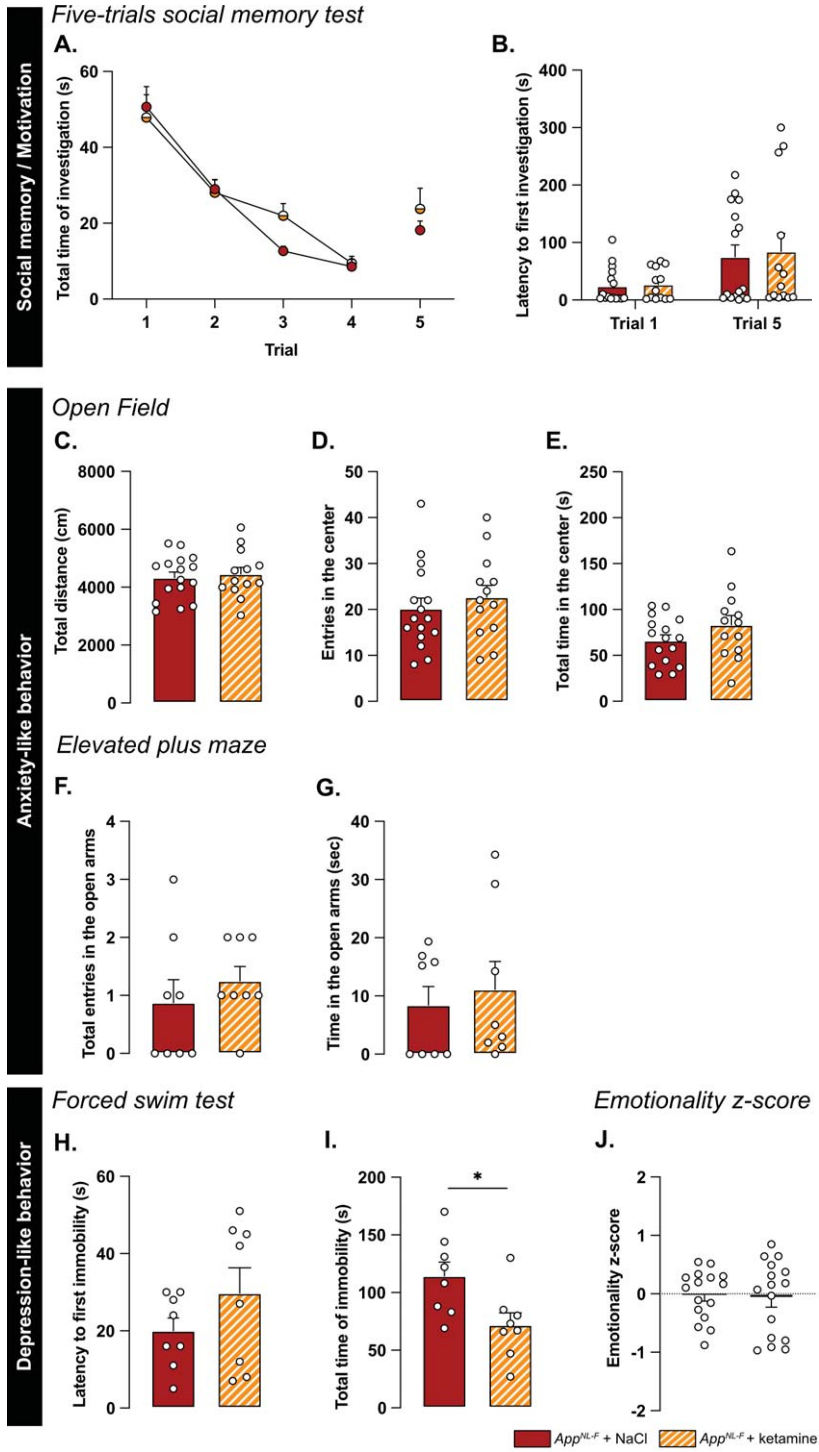App^{NL-F} + NaCl App^{NL-F} + ketamine

Fig. 6. (*Continued*)

in specific test for depressive-like behavior in these mice.

Ketamine (5 mg/kg) does not affect astrocyte morphology but partially restores synaptic dysfunctions and reduces astrocytic tonic inhibition

Astrocyte morphology was evaluated 24 h after ketamine (5 mg/kg) injection. The sholl analysis (Fig. 7A, B) did not unveil differences between NaCl and ketamine treated animals (Two-way ANOVA with distance and treatment as the main factors. Distance: $F_{(2.244,630.4)}=536.8$, $p<0.001$; Genotype: $F_{(1,181)}=0.5445$; $p=0.461$; Interaction: $F_{(19,5339)}=0.2808$, $p=0.999$). No differences were detected in the convex hull analysis (Fig. 7C) showing that a single injection of ketamine did not alter astrocytic morphology when given 24 h prior to analysis.

Regarding electrophysiological activity, no difference was observed on resting membrane potential (NaCl: -53.4 ± 3.08 mV, ketamine: -51.8 ± 5.29 mV; Fig. 7D) or any sEPSC parameters (Supplementary Figure 3M-P). However, ketamine induced a significant increase in frequency of mEPSC (NaCl: 0.10 ± 0.001 Hz, ketamine: 0.59 ± 0.11 Hz, $p<0.01$; Fig. 7E) while the amplitude (NaCl: -29.03 ± 4.40 pA, ketamine: -21.89 ± 3.52 pA; Fig. 7F), decay time (Supplementary Figure 3Q) and rise time (Supplementary Figure 3R) were not affected.

Synaptic plasticity deficits in 6-month-old App^{NL-F} mice were restored by ketamine: a subthreshold theta-burst stimulation gave an initial potentiation of the fEPSP in both conditions (NaCl:

1.32 ± 0.02, ketamine: 1.31 ± .11; Fig. 7G, H). Fifty-five minutes after stimulation, the magnitude of the long-term potentiation was significantly smaller in App^{NL-F} + ketamine compared to App^{NL-F} + NaCl (Fig. 7G-I; $p<0.001$). Taken together, these electrophysiological recordings confirm the ability of ketamine to retune misregulated synaptic transmission and plasticity.

Since we hypothesize that the synaptic mistuning in App^{NL-F} mice is mediated through astrocytes, we tested whether ketamine would affect the astrocytic tonic inhibition (Fig. 7J). Tonic GABA currents were recorded in hippocampal slices from App^{NL-F} mice that had been treated with ketamine 24 h earlier. Tonic GABA currents were significantly decreased in ketamine treated App^{NL-F} mice compared to saline treated group (3.94 ± 0.9 pA versus 32.11 ± 5.457 pA, $p<0.001$; Fig. 7K), suggesting a role for astrocytes in the antidepressant effect of ketamine.

DISCUSSION

As the final product of the dysregulated amyloid cascade, Aβ plaques have traditionally been studied as one of the main cause of AD pathology [52], although we know that both behavioral and pathophysiological changes occur before plaques can be detected [53]. In a late onset mouse model of AD (App^{NL-F}), at 6 months of age, limited occurrence of plaques has been reported [33] and we did not detect any Aβ plaques in the hippocampus in 6-month-old App^{NL-F} mice. However, an increase in non-soluble oligomers of Aβ was detected. Most importantly, at 6 months of age, App^{NL-F} mice have reactive-like astrocytes, increased tonic GABA, and

Fig. 7. **Synaptic mistuning but not astrocyte morphology is restored in App^{NL-F} by a single dose of ketamine (5 mg/kg).** A single injection of ketamine 24 h before immunohistochemistry analysis didn't affect the morphology of astrocytes. The sholl analysis unveiled a strong complexity from 7 to 25 μm from the nucleus (B). (A) depicts representative images from the two treatment conditions. Magenta: GFAP, cyan: DAPI; White arrows show a representative astrocyte. Scale bar for both view: 20 μm. The volume occupied by the cell (convex hull, C) remained unchanged after ketamine injection. App^{NL-F} + NaCl: 122 cells from three animals. App^{NL-F} + ketamine: 159 cells from four animals. Ketamine did not affect resting membrane potential in App^{NL-F} mice (D). In the same cell, the frequency of mEPSC is increased by ketamine treatment (E), whereas the amplitude of mEPSC remains unchanged (F). Mann-Whitney test: **$p<0.01$ statistically different as shown. App^{NL-F} + NaCl: $n=7$ cells recorded in five animals, App^{NL-F} + ketamine: $n=6$ cells recorded in six animals. With the same theta-burst (θ-burst) stimulation as previously used, the fEPSP magnitude goes back nearly to the baseline value in App^{NL-F} + ketamine mice whereas in the App^{NL-F} + NaCl, the stimulation triggers a long-term potentiation (G). Representative traces are shown on the top. There is no difference between the fEPSP magnitude in the two groups at 0–5 min after stimulation (H). However, at 55–60 min after the stimulation the fEPSP magnitude is significantly higher in NaCl treated mice compared to ketamine treated mice (I) Student *t*-test: ***$p<0.001$ statistically different as shown. App^{NL-F} + NaCl: $n=5$ recordings in four animals, App^{NL-F} + ketamine: $n=5$ recordings in four animals. Tonic GABA currents were recorded (J) and the average current was significantly reduced in App^{NL-F} mice treated with ketamine compared to NaCl treated mice (K). Mann-Whitney test ***$p<0.001$ significantly different as shown. App^{NL-F} + NaCl: $n=8$ cells recorded in four animals; App^{NL-F} + ketamine: $n=9$ cells recorded in four animals.
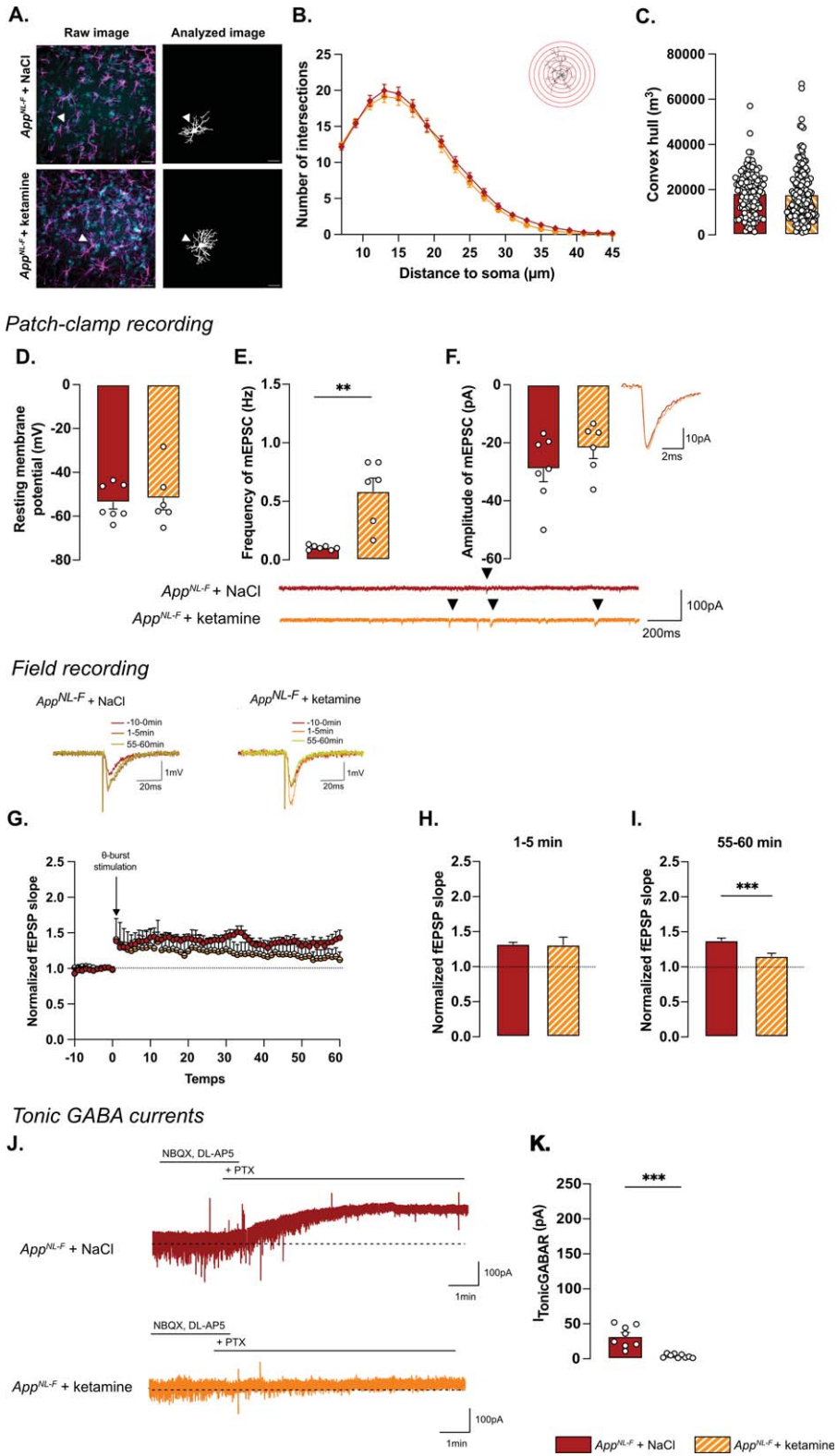
Fig. 7. (*Continued*)

synaptic misfunction. This is in good agreement with the hypothesis that Aβ oligomers are inducing several toxic events in early AD [54]. It is noteworthy that only male animals have been used in the present study. A recent study describes similarities and differences in behavior in male and female App^{NL-F} mice [46], however more work in this regard is needed. In particular, the effect of ketamine on female App^{NL-F} mice should be investigated since it has been shown that female wildtype mice are more sensitive to ketamine [55].

A reduced threshold for long-term potentiation in App^{NL-F} mice is a surprising finding. Memory impairments and dementia disorders have typically been associated with a decrease in synaptic potentiation; previous work in the App^{NL-F} mice at 6 months of age show no effect on LTP after a strong tetanic stimulation [56]. However, synaptic potentiation is not linearly correlated with memory, rather synaptic strength is constantly adjusted based on activity patterns in the neuronal network [57]. To learn and adapt to the changing environment, synaptic transmission needs to be plastic, while keeping the overall activity within optimal range. In fact, it has been proposed that cognitive deficits in early AD is not about reduced plasticity, but an imbalance at the network level [58], which is compatible with a reduced threshold for potentiation. Our results in the App^{NL-F} mice are consistent with previous work, where authors have been using a low or even sub-threshold stimulation protocol in other model with memory impairment [20]. The increase in synaptic potentiation, as well as the lack of change in evoked synaptic response, in 6-month-old App^{NL-F} mice has also been described by others [19], who attribute the effect to a decreased turnover of presynaptic proteins.

In this work we reveal that blocking MAO-B with deprenyl changes synaptic transmission in App^{NL-F} mice in several ways. As expected, deprenyl pretreatment increases the amplitude of synaptic events, both when evoked by spontaneous action potentials (sEPSC) and when arising from non-evoked release of individual vesicles (mEPSC). This effect is easily explained by an increase in membrane resistance due to the decreased GABA tone. In agreement, the frequency of mEPSC is increased in deprenyl-treated slices, however the frequency of sEPSC is not. Interestingly, the threshold for LTP is increased by blocking MAO-B and not reduced as one would expect with a reduced GABA tone. Thus, blocking GABA synthesis in astrocytes in App^{NL-F} mice entails more and other changes than a direct increase

in membrane resistance. It would be interesting for future studies to explore the mechanism underlying the apparent discrepancy between increased astrocytic tonic GABA and the reduced threshold for LTP. Previous work in our lab has shown that synaptic activity and plasticity are strongly interacting in a well-tuned relationship [44]. Thus, the increased synaptic activity induced by deprenyl could tune synaptic plasticity to specifically reverse synaptic deficits in the App^{NL-F} mice.

The synthesis and release of GABA from reactive astrocytes are well described phenomena and were first shown in a mouse model overexpressing App and with a severe plaque load [59]. Here we describe that astrocytes are reactive already in 6-month-old App^{NL-F} mice through a change in morphology as well as increased vimentin expression. As a consequence, and in line with previous research [41], tonic GABA is increased already before plaque formation in the App^{NL-F} mice model of AD. Reactive astrocytes [28] have been described as the starting point of several brain dysfunctions and proposed as an interesting therapeutic target in various brain disorders [60], and more recently in neurodegeneration and aging [61]. We do not directly rule out a neuronal origin of GABA that can be a consequence of excessive inhibitory activity and activation of extra synaptic $GABA_A$ receptors [62, 63]. However, the astrocytic origin of GABA is strongly supported by results showing that the main effect of blocking MAO-B in the hippocampus is a reduction in astrocytic GABA [42, 45].

Reactive astrocytes, as well as synaptic impairments, are linked to depressive-like behavior [64]. App^{NL-F} mice do indeed display depressive like behaviors in some tests already at 6 months. There is no test that directly translates to clinical depression, partly due to the fact that clinical depression can be describes as a syndrome, with different clinical presentations [65]. To get an overall vision of the emotional state of the App^{NL-F} mice, we compiled our behavioral data into an emotionality z-score, relevant to study depression-like behaviors assessed on different scales [66]. Since the reduced mobility could be another confounding factor in several of the tests used to assess depression-like behavior, data obtained in the open field and elevated plus maze were normalized with the travelled distance. When all the affective behavioral test are integrated in a z-score there is a significant difference in App^{NL-F} compared to C57Bl6 mice. This is in good agreement with early depressive symptoms observed in AD patients

[10] as well as results from other animals models of the disease [67]. Moreover, we confirm the lack of memory impairment at this age using the five-trials social memory test. In the last session of this test, the App^{NL-F} mice do not show increased time of interaction with the novel individual, as does the C57Bl6 mice. Having ruled out that the difference is due to olfactory problems or motor coordination problems, we suggest that this lack of interaction is due to a reduced social novelty interest, an indicator of an apathy-like behavior, which is consistent with the depressive like phenotype. However, another explanation could be that App^{NL-F} mice have deficits in social recognition consistent with recent observation in early diagnose patients [68]. We here use as the "presenting animal", mice with the same fur color, same age, same gender as the tested animal. Thus, App^{NL-F} mice might present early pattern separation deficits, as they cannot discriminate two very close situations (i.e., identify the mice as a new individual), in line with deficits observed in early AD [69]. Further work will need to be done to clarify this.

Ketamine was identified as a fast-acting antidepressant drug in the early 2000s [70] and has been suggested for treatment also in depression associated to AD [71, 72]. We investigated the therapeutic effect of a low dose of ketamine (5 mg/kg) delivered i.p., 24 h prior to experiments. In line with the literature [73], we successfully show the effect of this drug in the forced swim test and the splash test. There was no significant effect in the anxiety related tests and the overall emotionality z-score was not significantly improved. Moreover, the lack of exploration of the novel mice at the fifth trial in the social exploration test was not affected by ketamine.

The partial effect of ketamine on behavior contrasts with the significant effect of ketamine on the synaptic dysfunction in the App^{NL-F} mice, where mEPSC frequency is increased and the threshold for LTP induction is restored. In other models, especially when LTP is induced with a strong stimulation, ketamine has been shown to enhance LTP [74, 75]. Nevertheless, the reduction of LTP inducing threshold by ketamine is in good agreement with previous work from our lab where we show that ketamine affects synaptic transmission and plasticity in a state-dependent manner, to stabilize the synaptic tuning [44]. Therefore, caution should be exercised when comparing the impact of ketamine on synaptic function across various animal groups or treatment methods.

Thus, a single dose of ketamine partially corrects early synaptic dysfunctions, in the App^{NL-F} mice, but do not reverse behavioral deficits. However, ketamine does have an antidepressant effect in several of the tested paradigms. In this respect it is interesting to note that deprenyl, that also reverts synaptic dysfunctions in the App^{NL-F} mice is also used clinically as an anti-depressant drug [76], this effect has typically been ascribed to its effect on monoamine synthesis rather than the effect on astrocytes.

Increasing synchronous neuronal activity in the gamma frequency has been shown to slow-down disease progress and improve cognitive performance in AD [77] (but see also [78]). Moreover, recent work suggest that neuronal activity can indeed affect Aβ accumulation and plaque deposition [79]. Restoring synaptic transmission and plasticity may thus have a prophylactic effect on AD rather than an acute effect. It has been shown that depression is a risk factor for AD and interestingly antidepressant drugs seem to prevent the development if the disease [80] although the long term effect of ketamine in this regard has not been evaluated and whether this effect is mediated by retuning of synaptic function remains to be shown. We can however speculate that restoring synaptic tuning could also be a biological mechanism underlying the beneficial effect of a mental and physical active life-style [81]. Thus, it would be interesting to follow-up the long-term effect of chronic ketamine treatment, with its beneficial effect on synaptic tuning on the progression of AD.

Ketamine's mechanism of action is still debated. Interestingly, we see that ketamine and deprenyl have the same effects on synaptic transmission and plasticity in App^{NL-F} mice. Furthermore, we show that ketamine reduces tonic GABA, thus one possibility is that ketamine acts on reactive astrocytes to restabilize synaptic tuning, through changes in gliotransmission. This is in good agreement with recent results showing that ketamine affects astrocytic function [82], as well as astrocytic GABA metabolism [83]. Somewhat to our surprise, whilst morphology and function are generally considered to go hand in hand, ketamine did not affect astrocyte morphology after 24 h. This is consistent with the fact that GFAP expression is not reduced after ketamine treatment [84] and underscores the need of better understanding of what defines a reactive astrocyte [28].

Research on AD treatment has focused mainly on Aβ reducing treatments [85] or the cholinergic system [86]. Here we show that targeting the glutamatergic system can correct early synaptic

impairment as well as early depression-like behaviors observed in an AD model. How an early intervention restoring synaptic function affects the progression of AD remains to be shown.

AUTHOR CONTRIBUTIONS

ACKNOWLEDGMENTS

FUNDING

CONFLICT OF INTEREST

The authors have no conflict of interest to report.

DATA AVAILABILITY

All the data generated and analyzed in this study are included in the main manuscript. The custom macro used in the morphological analysis and the detailed statistics are available on reasonable request to the corresponding author.

SUPPLEMENTARY MATERIAL

The supplementary material is available in the electronic version of this article: https://dx.doi.org/10.3233/JAD-231461.

REFERENCES

[1] Ferri CP, Sousa R, Albanese E, Ribeiro WS, MHonyashiki M, Acosta D, Blom M, Dudgeon S, Frantz N, Geiger A, Jensen A, Ketteringham A, Kinnaird L, Martensson B, Rees G, Schaper F, Splaine M, Tami T, Westerlind K, Wortmann M (2009) *World Alzheimer's Report 2009*. Alzheimer's Disease International, London.

[2] Jahn H (2013) Memory loss in Alzheimer's disease. *Dialogues Clin Neurosci* **15**, 445-454.

[3] Shen LX, Yang YX, Kuo K, Li HQ, Chen SD, Chen KL, Dong Q, Tan L, Yu JT (2021) Social isolation, social interaction, and Alzheimer's disease: A Mendelian randomization study. *J Alzheimers Dis* **80**, 665-672.

[4] Zubenko GS, Zubenko WN, McPherson S, Spoor E, Marin DB, Farlow MR, Smith GE, Geda YE, Cummings JL, Petersen RC, Sunderland T (2003) A collaborative study of the emergence and clinical features of the major depressive syndrome of Alzheimer's disease. *Am J Psychiatry* **160**, 857-866.

[5] van Dyck CH, Swanson CJ, Aisen P, Bateman RJ, Chen C, Gee M, Kanekiyo M, Li D, Reyderman L, Cohen S, Froelich L, Katayama S, Sabbagh M, Vellas B, Watson D, Dhadda S, Irizarry M, Kramer LD, Iwatsubo T (2023) Lecanemab in early Alzheimer's disease. *N Engl J Med* **388**, 9-21.

[6] Naseri NN, Wang H, Guo J, Sharma M, Luo W (2019) The complexity of tau in Alzheimer's disease. *Neurosci Lett* **705**, 183-194.

[7] O'Brien RJ, Wong PC (2011) Amyloid precursor protein processing and Alzheimer's disease. *Annu Rev Neurosci* **34**, 185-204.

[8] Larson ME, Lesne SE (2012) Soluble Abeta oligomer production and toxicity. *J Neurochem* **120 Suppl 1**, 125-139.

[9] Matafora V, Gorb A, Yang F, Noble W, Bachi A, Perez-Nievas BG, Jimenez-Sanchez M (2023) Proteomics of the astrocyte secretome reveals changes in their response to soluble oligomeric Abeta. *J Neurochem* **166**, 346-366.

[10] Lyketsos CG, Carrillo MC, Ryan JM, Khachaturian AS, Trzepacz P, Amatniek J, Cedarbaum J, Brashear R, Miller DS (2011) Neuropsychiatric symptoms in Alzheimer's disease. *Alzheimers Dement* **7**, 532-539.

[11] Dafsari FS, Jessen F (2020) Depression-an underrecognized target for prevention of dementia in Alzheimer's disease. *Transl Psychiatry* **10**, 160.

[12] Pilozzi A, Foster S, Mischoulon D, Fava M, Huang X (2023) A brief review on the potential of psychedelics for treating Alzheimer's disease and related depression. *Int J Mol Sci* **24**, 12513.

[13] Manzoor S, Hoda N (2020) A comprehensive review of monoamine oxidase inhibitors as Anti-Alzheimer's disease agents: A review. *Eur J Med Chem* **206**, 112787.

[14] O'Dell RS, Higgins-Chen A, Gupta D, Chen MK, Naganawa M, Toyonaga T, Lu Y, Ni G, Chupak A, Zhao W, Salardini E, Nabulsi NB, Huang Y, Arnsten AFT, Carson RE, van Dyck CH, Mecca AP (2023) Principal component analysis of synaptic density measured with [(11)C]UCB-J PET in early Alzheimer's disease. *Neuroimage Clin* **39**, 103457.

[15] Scheff SW, Price DA, Schmitt FA, DeKosky ST, Mufson EJ (2007) Synaptic alterations in CA1 in mild Alzheimer disease and mild cognitive impairment. *Neurology* **68**, 1501-1508.

[16] Pusil S, López ME, Cuesta P, Bruña R, Pereda E, Maestú F (2019) Hypersynchronization in mild cognitive impairment: The 'X' model. *Brain* **142**, 3936-3950.

[17] Styr B, Slutsky I (2018) Imbalance between firing homeostasis and synaptic plasticity drives early-phase Alzheimer's disease. *Nat Neurosci* **21**, 463-473.

[18] Arroyo-Garcia LE, Isla AG, Andrade-Talavera Y, Balleza-Tapia H, Loera-Valencia R, Alvarez-Jimenez L, Pizzirusso G, Tambaro S, Nilsson P, Fisahn A (2021) Impaired spike-gamma coupling of area CA3 fast-spiking interneurons as the earliest functional impairment in the App(NL-G-F) mouse model of Alzheimer's disease. *Mol Psychiatry* **26**, 5557-5567.

[19] Hark TJ, Rao NR, Castillon C, Basta T, Smukowski S, Bao H, Upadhyay A, Bomba-Warczak E, Nomura T, O'Toole ET, Morgan GP, Ali L, Saito T, Guillermier C, Saido TC, Steinhauser ML, Stowell MHB, Chapman ER, Contractor A, Savas JN (2021) Pulse-chase proteomics of the App knockin mouse models of Alzheimer's disease reveals that synaptic dysfunction originates in presynaptic terminals. *Cell Syst* **12**, 141-158.e149.

[20] Loera-Valencia R, Vazquez-Juarez E, Munoz A, Gerenu G, Gomez-Galan M, Lindskog M, DeFelipe J, Cedazo-Minguez A, Merino-Serrais P (2021) High levels of 27-hydroxycholesterol results in synaptic plasticity alterations in the hippocampus. *Sci Rep* **11**, 3736.

[21] Wilkins RH, Brody IA (1969) Alzheimer's disease. *Arch Neurol* **21**, 109-110.

[22] De Bastiani MA, Bellaver B, Brum WS, Souza DG, Ferreira PCL, Rocha AS, Povala G, Ferrari-Souza JP, Benedet AL, Ashton NJ, Karikari TK, Zetterberg H, Blennow K, Rosa-Neto P, Pascoal TA, Zimmer ER, Alzheimer's Disease Neuroimaging Initiative (2023) Hippocampal GFAP-positive astrocyte responses to amyloid and tau pathologies. *Brain Behav Immun* **110**, 175-184.

[23] Choo IL, Carter SF, Scholl ML, Nordberg A (2014) Astrocytosis measured by (1)(1)C-deprenyl PET correlates with decrease in gray matter density in the parahippocampus of prodromal Alzheimer's patients. *Eur J Nucl Med Mol Imaging* **41**, 2120-2126.

[24] Fontana IC, Scarpa M, Malarte ML, Rocha FM, Auselle-Bosch S, Bluma M, Bucci M, Chiotis K, Kumar A, Nordberg A (2023) Astrocyte signature in Alzheimer's disease continuum through a multi-PET tracer imaging perspective. *Cells* **12**, 1469.

[25] Benedet AL, Mila-Aloma M, Vrillon A, Ashton NJ, Pascoal TA, Lussier F, Karikari TK, Hourregue C, Cognat E, Dumurgier J, Stevenson J, Rahmouni N, Pallen V, Poltronetti NM, Salvado G, Shekari M, Operto G, Gispert JD, Minguillon C, Fauria K, Kollmorgen G, Suridjan I, Zimmer ER, Zetterberg H, Molinuevo JL, Paquet C, Rosa-Neto P, Blennow K, Suarez-Calvet M, Translational Biomarkers in Aging and Dementia (TRIAD) study, Alzheimer's and Families (ALFA) study, and BioCogBank Paris Lariboisière cohort (2021) Differences between plasma and cerebrospinal fluid glial fibrillary acidic protein levels across the Alzheimer disease continuum. *JAMA Neurol* **78**, 1471-1483.

[26] Zhao J, O'Connor T, Vassar R (2011) The contribution of activated astrocytes to Abeta production: Implications for Alzheimer's disease pathogenesis. *J Neuroinflammation* **8**, 150.

[27] Brandebura AN, Paumier A, Onur TS, Allen NJ (2023) Astrocyte contribution to dysfunction, risk and progression in neurodegenerative disorders. *Nat Rev Neurosci* **24**, 23-39.

[28] Escartin C, Galea E, Lakatos A, O'Callaghan JP, Petzold GC, Serrano-Pozo A, Steinhäuser C, Volterra A, Carmignoto G, Agarwal A, Allen NJ, Araque A, Barbeito L, Barzilai A, Bergles DE, Bonvento G, Butt AM, Chen W-T, Cohen-Salmon M, Cunningham C, Deneen B, De Strooper B, Díaz-Castro B, Farina C, Freeman M, Gallo V, Goldman JE, Goldman SA, Götz M, Gutiérrez A, Haydon PG, Heiland DH, Hol EM, Holt MG, Iino M, Kastanenka KV, Kettenmann H, Khakh BS, Koizumi S, Lee CJ, Liddelow SA, MacVicar BA, Magistretti P, Messing A, Mishra A, Molofsky AV, Murai KK, Norris CM, Okada S, Oliet SHR, Oliveira JF, Panatier A, Parpura V, Pekna M, Pekny M, Pellerin L, Perea G, Pérez-Nievas BG, Pfrieger FW, Poskanzer KE, Quintana FJ, Ransohoff RM, Riquelme-Perez M, Robel S, Rose CR, Rothstein JD, Rouach N, Rowitch DH, Semyanov A, Sirko S, Sontheimer H, Swanson RA, Vitorica J, Wanner I-B, Wood LB, Wu J, Zheng B, Zimmer ER, Zorec R, Sofroniew MV, Verkhratsky A (2021) Reactive astrocyte nomenclature, definitions, and future directions. *Nat Neurosci* **24**, 312-325.

[29] Ekblom J, Jossan SS, Bergstrom M, Oreland L, Walum E, Aquilonius SM (1993) Monoamine oxidase-B in astrocytes. *Glia* **8**, 122-132.

[30] Yoon BE, Lee CJ (2014) GABA as a rising gliotransmitter. *Front Neural Circuits* **8**, 141.

[31] Esquerda-Canals G, Montoliu-Gaya L, Guell-Bosch J, Villegas S (2017) Mouse models of Alzheimer's disease. *J Alzheimers Dis* **57**, 1171-1183.

[32] Sasaguri H, Nilsson P, Hashimoto S, Nagata K, Saito T, De Strooper B, Hardy J, Vassar R, Winblad B, Saido TC (2017) APP mouse models for Alzheimer's disease preclinical studies. *EMBO J* **36**, 2473-2487.

[33] Saito T, Matsuba Y, Mihira N, Takano J, Nilsson P, Itohara S, Iwata N, Saido TC (2014) Single App knock-in mouse models of Alzheimer's disease. *Nat Neurosci* **17**, 661-663.

[34] Nilsson P, Saito T, Saido TC (2014) New mouse model of Alzheimer's. *ACS Chem Neurosci* **5**, 499-502.

[35] Saito T, Mihira N, Matsuba Y, Sasaguri H, Hashimoto S, Narasimhan S, Zhang B, Murayama S, Higuchi M, Lee VMY, Trojanowski JQ, Saido TC (2019) Humanization of the entire murine Mapt gene provides a murine model of pathological human tau propagation. *J Biol Chem* **294**, 12754-12765.

[36] Jiang R, Shimozawa M, Mayer J, Tambaro S, Kumar R, Abelein A, Winblad B, Bogdanovic N, Nilsson P (2022) Autophagy impairment in App knock-in Alzheimer's model mice. *Front Aging Neurosci* **14**, 878303.

[37] Leal NS, Dentoni G, Schreiner B, Naia L, Piras A, Graff C, Cattaneo A, Meli G, Hamasaki M, Nilsson P, Ankarcrona M (2020) Amyloid beta-peptide increases mitochondria-endoplasmic reticulum contact altering mitochondrial function and autophagosome formation in Alzheimer's disease-related models. *Cells* **9**, 2552.

[38] Naia L, Shimozawa M, Bereczki E, Li X, Liu J, Jiang R, Giraud R, Leal NS, Pinho CM, Berger E, Falk VL, Dentoni G, Ankarcrona M, Nilsson P (2023) Mitochondrial hypermetabolism precedes impaired autophagy and synaptic disorganization in App knock-in Alzheimer mouse models. *Mol Psychiatry* **28**, 3966-3981.

[39] Petrache AL, Rajulawalla A, Shi A, Wetzel A, Saito T, Saido TC, Harvey K, Ali AB (2019) Aberrant excitatory-inhibitory synaptic mechanisms in entorhinal cortex microcircuits during the pathogenesis of Alzheimer's disease. *Cereb Cortex* **29**, 1834-1850.

[40] Guilloux JP, Seney M, Edgar N, Sibille E (2011) Integrated behavioral z-scoring increases the sensitivity and reliability of behavioral phenotyping in mice: Relevance to emotionality and sex. *J Neurosci Methods* **197**, 21-31.

[41] Lee S, Yoon BE, Berglund K, Oh SJ, Park H, Shin HS, Augustine GJ, Lee CJ (2010) Channel-mediated tonic GABA release from glia. *Science* **330**, 790-796.

[42] Srivastava I, Vazquez-Juarez E, Henning L, Gomez-Galan M, Lindskog M (2020) Blocking astrocytic GABA restores synaptic plasticity in prefrontal cortex of rat model of depression. *Cells* **9**, 1705.

[43] Berg S, Kutra D, Kroeger T, Straehle CN, Kausler BX, Haubold C, Schiegg M, Ales J, Beier T, Rudy M, Eren K, Cervantes JI, Xu B, Beuttenmueller F, Wolny A, Zhang C, Koethe U, Hamprecht FA, Kreshuk A (2019) ilastik: Interactive machine learning for (bio)image analysis. *Nat Methods* **16**, 1226-1232.

[44] Vazquez-Juarez E, Srivastava I, Lindskog M (2023) The effect of ketamine on synaptic mistuning induced by impaired glutamate reuptake. *Neuropsychopharmacology* **48**, 1859-1868.

[45] Yoon BE, Woo J, Chun YE, Chun H, Jo S, Bae JY, An H, Min JO, Oh SJ, Han KS, Kim HY, Kim T, Kim YS, Bae YC, Lee CJ (2014) Glial GABA, synthesized by monoamine oxidase B, mediates tonic inhibition. *J Physiol* **592**, 4951-4968.

[46] Britz J, Ojo E, Dhukhwa A, Saito T, Saido TC, Hascup ER, Hascup KN, Tischkau SA (2022) Assessing sex-specific circadian, metabolic, and cognitive phenotypes in the AbetaPP/PS1 and APPNL-F/NL-F models of Alzheimer's disease. *J Alzheimers Dis* **85**, 1077-1093.

[47] Dominguez S, Rey CC, Therreau L, Fanton A, Massotte D, Verret L, Piskorowski RA, Chevaleyre V (2019) Maturation of PNN and ErbB4 signaling in area CA2 during adolescence underlies the emergence of PV interneuron plasticity and social memory. *Cell Rep* **29**, 1099-1112 e1094.

[48] Leroy F, Brann DH, Meira T, Siegelbaum SA (2017) Input-timing-dependent plasticity in the hippocampal CA2 region and its potential role in social memory. *Neuron* **95**, 1089-1102.e5.

[49] Rey CC, Robert V, Bouisset G, Loisy M, Lopez S, Cattaud V, Lejards C, Piskorowski RA, Rampon C, Chevaleyre V, Verret L (2022) Altered inhibitory function in hippocampal CA2 contributes in social memory deficits in Alzheimer's mouse model. *iScience* **25**, 103895.

[50] Deardorff WJ, Grossberg GT (2019) Behavioral and psychological symptoms in Alzheimer's dementia and vascular dementia. *Handb Clin Neurol* **165**, 5-32.

[51] Pham TH, Gardier AM (2019) Fast-acting antidepressant activity of ketamine: Highlights on brain serotonin, glutamate, and GABA neurotransmission in preclinical studies. *Pharmacol Ther* **199**, 58-90.

[52] Selkoe DJ, Hardy J (2016) The amyloid hypothesis of Alzheimer's disease at 25 years. *EMBO Mol Med* **8**, 595-608.

[53] Gouilly D, Rafiq M, Nogueira L, Salabert AS, Payoux P, Péran P, Pariente J (2023) Beyond the amyloid cascade: An update of Alzheimer's disease pathophysiology. *Rev Neurol (Paris)* **179**, 812-830.

[54] Sciaccaluga M, Megaro A, Bellomo G, Ruffolo G, Romoli M, Palma E, Costa C (2021) An unbalanced synaptic transmission: Cause or consequence of the amyloid oligomers neurotoxicity? *Int J Mol Sci* **22**, 5991.

[55] Franceschelli A, Sens J, Herchick S, Thelen C, Pitychoutis PM (2015) Sex differences in the rapid and the sustained antidepressant-like effects of ketamine in stress-naïve and "depressed" mice exposed to chronic mild stress. *Neuroscience* **290**, 49-60.

[56] Benitez DP, Jiang S, Wood J, Wang R, Hall CM, Peerboom C, Wong N, Stringer KM, Vitanova KS, Smith VC, Joshi D, Saito T, Saido TC, Hardy J, Hanrieder J, De Strooper B, Salih DA, Tripathi T, Edwards FA, Cummings DM (2021) Knock-in models related to Alzheimer's disease: Synaptic transmission, plaques and the role of microglia. *Mol Neurodegen* **16**, 47.

[57] Neves G, Cooke SF, Bliss TV (2008) Synaptic plasticity, memory and the hippocampus: A neural network approach to causality. *Nat Rev Neurosci* **9**, 65-75.

[58] Frere S, Slutsky I (2018) Alzheimer's disease: From firing instability to homeostasis network collapse. *Neuron* **97**, 32-58.

[59] Jo S, Yarishkin O, Hwang YJ, Chun YE, Park M, Woo DH, Bae JY, Kim T, Lee J, Chun H, Park HJ, Lee DY, Hong J, Kim HY, Oh SJ, Park SJ, Lee H, Yoon BE, Kim Y, Jeong Y, Shim I, Bae YC, Cho J, Kowall NW, Ryu H, Hwang E, Kim D, Lee CJ (2014) GABA from reactive astrocytes impairs memory in mouse models of Alzheimer's disease. *Nat Med* **20**, 886-896.

[60] Liddelow SA, Barres BA (2017) Reactive astrocytes: Production, function, and therapeutic potential. *Immunity* **46**, 957-967.

[61] Patani R, Hardingham GE, Liddelow SA (2023) Functional roles of reactive astrocytes in neuroinflammation and neurodegeneration. *Nat Rev Neurol* **19**, 395-409.

[62] Farrant M, Kaila K (2007) The cellular, molecular and ionic basis of GABA(A) receptor signalling. *Prog Brain Res* **160**, 59-87.

[63] Song I, Savtchenko L, Semyanov A (2011) Tonic excitation or inhibition is set by GABA(A) conductance in hippocampal interneurons. *Nat Commun* **2**, 376.

[64] Wang Y, Ni J, Zhai L, Gao C, Xie L, Zhao L, Yin X (2019) Inhibition of activated astrocyte ameliorates lipopolysaccharide- induced depressive-like behaviors. *J Affect Disord* **242**, 52-59.

[65] Soderlund J, Lindskog M (2018) Relevance of rodent models of depression in clinical practice: Can we overcome the obstacles in translational neuropsychiatry? *Int J Neuropsychopharmacol* **21**, 668-676.

[66] Portal B, Vasile F, Zapata J, Lejards C, Ait Tayeb AEK, Colle R, Verstuyft C, Corruble E, Rouach N, Guiard BP (2022) Astroglial connexins inactivation increases relapse of depressive-like phenotype after antidepressant withdrawal. *Int J Mol Sci* **23**, 13227.

[67] Yan L, Li L, Han W, Pan B, Xue X, Mei B (2013) Age-related neuropsychiatric symptoms in presenilins conditional double knockout mice. *Brain Res Bull* **97**, 104-111.

[68] Strijkert F, Huitema RB, van Munster BC, Spikman JM (2023) Impaired emotion recognition: A potential marker for social behavioral problems in patients with amnestic mild cognitive impairment and early Alzheimer disease? *Alzheimer Dis Assoc Disord* **37**, 189-194.

[69] Parizkova M, Lerch O, Andel R, Kalinova J, Markova H, Vyhnalek M, Hort J, Laczo J (2020) Spatial pattern separation in early Alzheimer's disease. *J Alzheimers Dis* **76**, 121-138.

[70] Berman RM, Cappiello A, Anand A, Oren DA, Heninger GR, Charney DS, Krystal JH (2000) Antidepressant effects of ketamine in depressed patients. *Biol Psychiatry* **47**, 351-354.

[71] Smalheiser NR (2019) Ketamine: A neglected therapy for Alzheimer disease. *Front Aging Neurosci* **11**, 186.

[72] Mohammad Shehata I, Masood W, Nemr N, Anderson A, Bhusal K, Edinoff AN, Cornett EM, Kaye AM, Kaye AD (2022) The possible application of ketamine in the treatment of depression in Alzheimer's disease. *Neurol Int* **14**, 310-321.

[73] Abdallah CG, Sanacora G, Duman RS, Krystal JH (2018) The neurobiology of depression, ketamine and rapid-acting antidepressants: Is it glutamate inhibition or activation? *Pharmacol Ther* **190**, 148-158.

[74] Zhu X, Zhang F, You Y, Wang H, Yuan S, Wu B, Zhu R, Liu D, Yan F, Wang Z (2023) S-ketamine exerts antidepressant effects by regulating Rac1 GTPase mediated synaptic plasticity in the hippocampus of stressed rats. *Cell Mol Neurobiol* **43**, 299-314.

[75] Aleksandrova LR, Wang YT, Phillips AG (2020) Ketamine and its metabolite, (2R,6R)-HNK, restore hippocampal LTP and long-term spatial memory in the Wistar-Kyoto rat model of depression. *Mol Brain* **13**, 92.

[76] Rossano F, Caiazza C, Sobrino A, Solini N, Vellucci A, Zotti N, Fornaro M, Gillman K, Cattaneo CI, Van den Eynde V, Birkenhager TK, Ruhé HG, Stahl S, Iasevoli F, de Bartolomeis A (2023) Efficacy and safety of selegiline across different psychiatric disorders: A systematic review and meta-analysis of oral and transdermal formulations. *Eur Neuropsychopharmacol* **72**, 60-78.

[77] Martorell AJ, Paulson AL, Suk HJ, Abdurrob F, Drummond GT, Guan W, Young JZ, Kim DN, Kritskiy O, Barker SJ, Mangena V, Prince SM, Brown EN, Chung K, Boyden ES, Singer AC, Tsai LH (2019) Multi-sensory gamma stimulation ameliorates Alzheimer's-associated pathology and improves cognition. *Cell* **177**, 256-271.e22.

[78] Soula M, Martin-Avila A, Zhang Y, Dhingra A, Nitzan N, Sadowski MJ, Gan WB, Buzsaki G (2023) Forty-hertz light stimulation does not entrain native gamma oscillations in Alzheimer's disease model mice. *Nat Neurosci* **26**, 570-578.

[79] Bero AW, Yan P, Roh JH, Cirrito JR, Stewart FR, Raichle ME, Lee J-M, Holtzman DM (2011) Neuronal activity regulates the regional vulnerability to amyloid-β deposition. *Nat Neurosci* **14**, 750-756.

[80] Kessing LV, Søndergård L, Forman JL, Andersen PK (2009) Antidepressants and dementia. *J Affect Disord* **117**, 24-29.

[81] Janssen N, Handels RL, Wimo A, Antikainen R, Laatikainen T, Soininen H, Strandberg T, Tuomilehto J, Kivipelto M, Evers S, Verhey FRJ, Ngandu T (2022) Association between cognition, health related quality of life, and costs in a population at risk for cognitive decline. *J Alzheimers Dis* **89**, 623-632.

[82] Stenovec M, Li B, Verkhratsky A, Zorec R (2020) Astrocytes in rapid ketamine antidepressant action. *Neuropharmacology* **173**, 108158.

[83] Tang XH, Diao YG, Ren ZY, Zang YY, Zhang GF, Wang XM, Duan GF, Shen JC, Hashimoto K, Zhou ZQ, Yang JJ (2023) A role of GABA(A) receptor alpha1 subunit in the hippocampus for rapid-acting antidepressant-like effects of ketamine. *Neuropharmacology* **225**, 109383.

[84] Ma X, Yang S, Zhang Z, Liu L, Shi W, Yang S, Li S, Cai X, Zhou Q (2022) Rapid and sustained restoration of astrocytic functions by ketamine in depression model mice. *Biochem Biophys Res Commun* **616**, 89-94.

[85] Yang P, Sun F (2021) Aducanumab: The first targeted Alzheimer's therapy. *Drug Discov Ther* **15**, 166-168.

[86] Sharma K (2019) Cholinesterase inhibitors as Alzheimer's therapeutics (Review). *Mol Med Rep* **20**, 1479-1487.